

# UCLA

## UCLA Previously Published Works

### Title

Reprogramming the Tolerogenic Immune Response Against Pancreatic Cancer Metastases by Lipid Nanoparticles Delivering a STING Agonist Plus Mutant KRAS mRNA.

### Permalink

<https://escholarship.org/uc/item/0kb242r8>

### Journal

ACS Nano, 19(9)

### Authors

Xu, Xiao

Wang, Xiang

Liao, Yu-Pei

et al.

### Publication Date

2025-03-11

### DOI

10.1021/acsnano.4c14102

Peer reviewed

# Reprogramming the Tolerogenic Immune Response Against Pancreatic Cancer Metastases by Lipid Nanoparticles Delivering a STING Agonist Plus Mutant KRAS mRNA

Xiao Xu, Xiang Wang, Yu-Pei Liao, Lijia Luo, and Andre E. Nel\*



Cite This: *ACS Nano* 2025, 19, 8579–8594



Read Online

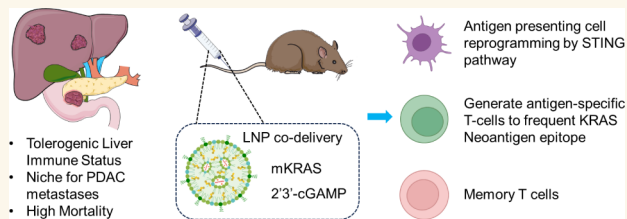
ACCESS |

Metrics & More

Article Recommendations

Supporting Information

**ABSTRACT:** We demonstrate reprogramming of the tolerogenic immune environment in the liver for mounting an effective immune response against often-fatal pancreatic cancer metastases. This was achieved by engineering a lipid nanoparticle (LNP) to deliver mRNA encoding the KRAS G12D neoantigenic epitope along with cGAMP, a dinucleotide agonist of the stimulator of the interferon genes (STING) pathway, capable of activating a type I interferon response. cGAMP/mKRAS/LNP were synthesized by a microfluidics approach involving nanoprecipitation of mRNA and cGAMP by an ionizable lipid, MC3. Controls included nanoparticles delivering individual components or a wild-type RAS sequence. The dual delivery carrier successfully activated the type I interferon pathway *in vitro* as well as *in vivo*, with reprogramming of costimulatory receptor (CD80 and CD86) and MHC-I expression on liver antigen-presenting cells (APC). This allowed the generation of IFN- $\gamma$  producing cytotoxic T cells, capable of mounting an effective immune response in the metastatic KRAS pancreatic cancer (KPC) mouse model. Noteworthy, intravenous injection of cGAMP/mKRAS/LNP suppressed metastatic growth significantly and prolonged animal survival, both prophylactically and during treatment of established metastases. The protective immune response was mediated by the generation of perforin-releasing CD8<sup>+</sup> cytotoxic T cells, engaged in pancreatic cancer cell killing. Importantly, the immune response could also be adoptively transferred by injecting splenocytes (containing memory T cells) from treated into nontreated recipient mice. This study demonstrates that reprogramming the immune-protective niche for metastatic pancreatic cancer can be achieved by the delivery of a STING agonist and mutant KRAS mRNA via ionizable LNPs, offering both prophylactic and therapeutic advantages.



**KEYWORDS:** lipid nanoparticles, mRNA delivery, cancer vaccine, pancreatic cancer, liver metastasis

## INTRODUCTION

Pancreatic ductal adenocarcinoma (PDAC) remains a formidable challenge in oncology, with a dismal 5-year survival rate of only 12%.<sup>1</sup> The disease typically presents at an advanced stage, often accompanied by metastasis to the liver, lungs, and peritoneum.<sup>2</sup> Among these, hepatic metastasis is particularly lethal, regardless of the primary tumor's therapeutic response.<sup>3</sup> The poor prognosis is attributed to the liver's immune-tolerant environment, which is shaped by the production of immunosuppressive cytokines such as TGF- $\beta$  and IL-10, and the presence of tolerogenic APCs, including liver sinusoidal endothelial cells (LSECs), Kupffer cells, and immature dendritic cells (DCs).<sup>4–6</sup> Additionally, the liver's rich blood flow within the sinusoidal circulation supplies copious nutrients that facilitate tumor growth. This paper aims to present a novel strategy for reprogramming the liver's

immune microenvironment using LNPs to deliver a STING pathway agonist. This approach is combined with the use of a commonly expressed KRAS neoantigen to activate cytotoxic T-cells, thereby enhancing the immune response against PDAC.

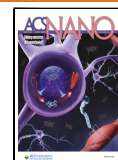
To advance immunotherapy for PDAC metastasis to the liver, we were interested in 4 common KRAS mutations (G12D, G12V, G12R, and G13D) that appear in >90% of PDAC patients,<sup>1,7</sup> as potential neoantigen epitopes that can be considered for combination with a STING agonist in LNPs.<sup>8</sup>

**Received:** October 7, 2024

**Revised:** February 14, 2025

**Accepted:** February 18, 2025

**Published:** March 3, 2025



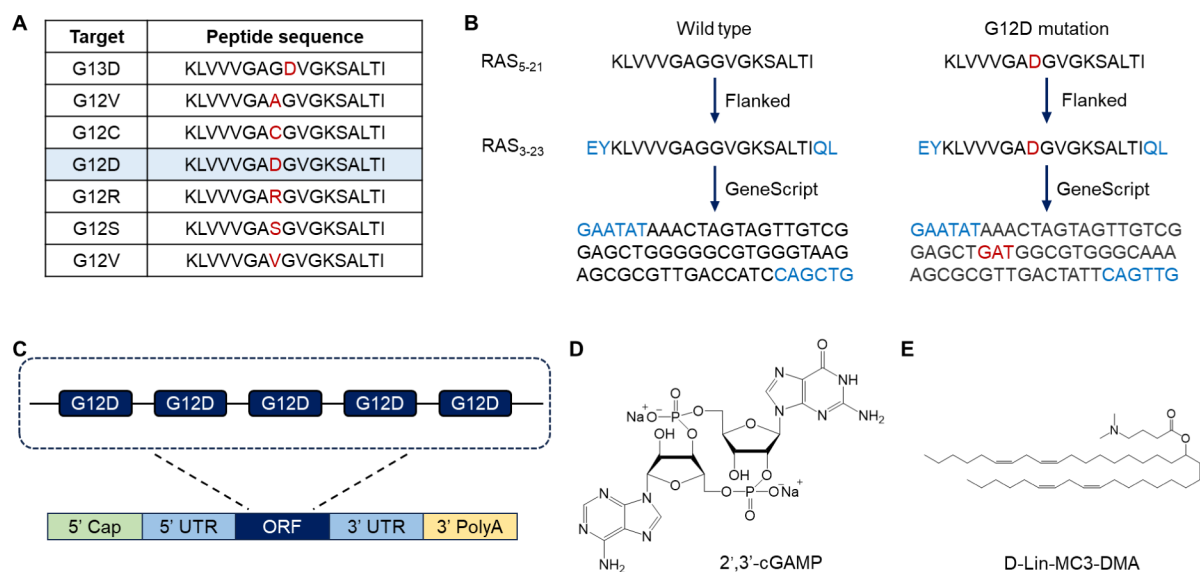


**Figure 1.** mRNA design and chemistry of cGAMP and D-Lin-MC3-DMA. (A) Common KRAS mutant sequences, including for the wild-type 17-peptide RAS<sub>5-21</sub> sequence. (B) Comparison of wild-type RAS<sub>5-21</sub> and G12D mutant KRAS<sub>5-21</sub>, used for mRNA design by including 2 amino acids upstream and downstream as flanking sequences, before reverse translation into the respective nucleic acid sequences by the online GeneScript tool. (C) The open-reading frame included 5 repetitions of each nucleotide sequence, with the addition of start codon and stop codons, 5' Cap, 5' UTR, 3' UTR, and a 3' PolyA tail. (D) Structure of 2',3'-cGAMP. (E) Structure of D-Lin-MC3-DMA lipid.

Among these mutations, G12D is the most prevalent, found in 35% of PDAC patients.<sup>9</sup> It is a major oncogenic driver that is also frequently used in the orthotopic PDAC cancer model we developed for simulating several human PDAC characteristics. The use of KRAS mutant peptides for PDAC immunotherapy and providing a vaccination attempt against the return PDAC has progressed to clinical trials, as shown, for instance, by the TG01 peptide cocktail that has been combined with granulocyte-macrophage colony-stimulating factor (GM-CSF) for intervention in pancreatic cancer.<sup>10</sup> Additionally, mRNA vaccine technology, which gained prominence during the COVID-19 pandemic,<sup>11</sup> has made significant inroads into cancer immunology.<sup>12-16</sup> For instance, Moderna's mRNA-5671 (V941) encapsulates mRNA strands encoding KRAS mutations G12D, G12V, G13D, or G12C in LNPs for the treatment of nonsmall cell lung cancer, colorectal cancers, or pancreatic adenocarcinoma.<sup>17</sup> To address the impact of the tolerogenic immune landscape in the liver, which facilitates the metastasis of PDAC, we explored an alternative KRAS-targeting strategy. This approach involves the encapsulation of mRNA encoding the KRAS G12D neoantigen together with the cyclic dinucleotide cGAMP, a potent STING agonist, to reprogram the tolerogenic liver microenvironment in a metastatic KPC model.<sup>18</sup> To the best of our knowledge, this approach has not been explored in the Moderna studies or in the TG01 peptide vaccine cocktail. As such, it represents a promising strategy to enhance KRAS-specific vaccination efforts and overcome immunosuppressive barriers in the liver.

We have previously demonstrated the effectiveness of liver-targeting cationic LNPs for encapsulating mRNA strands that encode multiple food allergen epitopes.<sup>6</sup> This approach enables targeted delivery to liver APCs, capable of promoting a tolerogenic immune response that mitigates peanut anaphylaxis.<sup>6</sup> This includes the tolerogenic contribution of Kupffer cells and LSECs in the generation of regulatory T cells (Tregs) that suppress the allergic inflammatory response to crude peanut allergen proteins. Moreover, it is likely that the

same tolerogenic APCs and Tregs contribute to the immune suppressive effects that provide a protective niche that facilitates PDAC metastatic spread.<sup>19,20</sup> Therefore, we hypothesized that reprogramming the tolerogenic immune environment in the liver is a unique strategy to generate an anti-PDAC immune response against the immunogenic KRAS G12D mutant. To achieve a cytotoxic rather than a tolerogenic response, this requires additional cargo to switch the tolerogenic response to a protective immune response in the liver. The STING pathway was chosen for its robust ability to activate anticancer T cell immunity by a cyclic dinucleotide that can also be coprecipitated with mRNA.<sup>15,16,21-23</sup> Since cGAMP is a strong inducer of the type I interferon pathway, it provides a means of generating robust cytotoxic T cell responses by uptake in liver APCs.<sup>24,25</sup> Indeed, it has been shown that the conjugation of cGAMP to a PEGylated lipid enables nano disc incorporation and generation of robust antitumor immunity in colorectal and breast cancer models.<sup>26</sup>

Building on this background, we designed and synthesized liver-targeting ionizable LNPs, dual-loaded with mRNA encoding a KRAS G12D epitope plus the STING agonist, cGAMP. After confirming that these particles are efficiently taken up by liver nonparenchymal cells (NPCs) following intravenous (IV) administration, we demonstrated activation of the type I interferon pathway in liver APCs, as well as the generation of IFN- $\gamma$ -producing T cells in ELISPOT assays. Using a metastatic PDAC model with KPC cells, we demonstrate that this dual delivery strategy is capable of effectively suppressing metastatic tumor cell growth by cytotoxic CD8<sup>+</sup> T cells, generated prophylactically, or following the establishment of liver metastases. Additionally, the ability of the treatment to generate memory T cells could be used for adoptive transfer to protect naïve recipients receiving KPC hemisplenic injection. Overall, this study presents a novel approach for overcoming the immunological challenges of PDAC liver metastasis using a cationic LNP-based vaccination strategy.

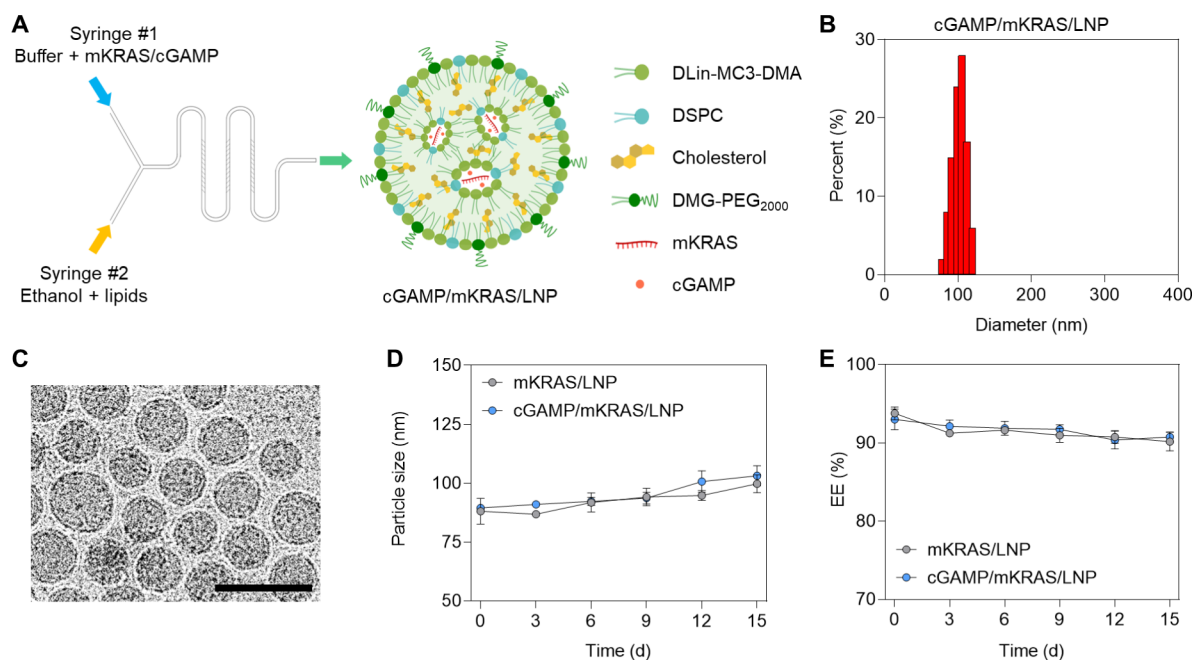


**Figure 2.** Preparation and characterization of LNP. (A) LNP with cGAMP and KRAS G12D mRNA cargo were prepared by blending the organic phase, containing the lipids MC3, DSPC, cholesterol, and DMG-PEG<sub>2000</sub>, with the aqueous phase containing cGAMP and mKRAS in a microfluidics blender. The cGAMP/mKRAS/LNP were dialysis against PBS at 4 °C for 1 h before filtering (220 nm). (B) The particle size, PDI, and surface charge of cGAMP/mKRAS/LNP were  $91.6 \pm 0.4$  nm,  $0.173 \pm 0.012$ , and  $-2.4 \pm 1.2$  mV, respectively. (C) Representative cryoEM image of cGAMP/mKRAS/LNP. Scale bar is 100 nm. (D) Change of particle size during storage at 4 °C for 15 days. (E) Change of EE during storage at 4 °C for 15 days.

## RESULTS

### LNP Preparation for Delivery of cGAMP and KRAS G12D mRNA Combinations.

We have previously demonstrated that tolerogenic liver APCs can be targeted by cationic LNPs to induce tolerogenic immune responses to food allergens by including selected T cell epitopes that promote Tregs-mediated suppression of allergic reactions.<sup>6</sup> This outcome was achieved by particles constructed with the ionizable lipid component, D-Lin-MC3-DMA (MC3), which allows uptake by a range of parenchymal and nonparenchymal liver cell types. This uptake can be further enhanced in the APCs by decorating the particle surface with a mannose ligand.<sup>6,27</sup> In this study, we hypothesized that the tolerogenic effects of liver APCs could be reprogrammed using a STING agonist to develop a protective cytotoxic T cell response against a KRAS neoepitope, thereby reversing the immune protective niche facilitating pancreatic cancer metastasis to the liver. We focused on the KRAS G12D epitope, which is expressed in 35% of human PDAC cases and is also present in the robust transgenic *Kras<sup>LSL</sup> G12D/+; Trp53<sup>LSL</sup> R172H/+; and Pdx-1-Cre* mouse model, which allowed us to develop an orthotopic KPC mouse model (Figure 1A).<sup>18</sup> The KRAS G12D peptide sequence (aa 3–23) was used to derive the corresponding cDNA sequence (Figure 1B), followed by the insertion of five copies into an open reading frame, flanked by natural amino acid sequences (Figure 1C). A five-epitope repetition was used to enhance the likelihood of effective MHC class I presentation, thereby increasing immunogenicity. Additionally, we constructed a control cDNA sequence incorporating five repeats of a corresponding nonimmunogenic peptide sequence from wild-type RAS (aa 5–21), also flanked by natural amino acid sequences (Figure 1B). Following the addition of start and stop codons, codon optimization was

performed using the online GeneScript tool, yielding GC contents of 52.08% and 53.65% for the KRAS and RAS<sup>WT</sup> strands, respectively (Figure S1A). These optimized cDNA sequences were used to order the corresponding mRNA strands from TriLink Biotechnologies, which delivered 582-nucleotide-long strands (Figure S1B).

To construct an ionizable LNP that coencapsulates a STING agonist with mRNA, we selected a negatively charged 2′/3′-cGAMP dinucleotide sequence (Figure 1D) for electrostatic binding to the cationic lipid, MC3, which was also used for the nanoprecipitation of the mRNA (Figure 1E). The LNP synthesis was conducted using a microfluidic mixer (Nano-assemblr), with negatively charged mRNA and cGAMP introduced in a diluted acetic acid buffer in one channel, while the ethanol-diluted lipid mixture was infused into the second channel (Figure 2A). Details of the analyte concentrations and volume calculations for microfluidic synthesis appear in Figure S2. Following dialysis and particle filtration, dynamic light scattering analysis showed average particle sizes of 91.6 nm (Figure 2B) with a polydispersity index (PDI) of 0.173. cryoEM imaging confirmed the synthesis of spherical particles, displaying a nanoprecipitated complex (Figure 2C). The concentrations of cGAMP and mKRAS were quantified using a cGAMP ELISA kit and a RiboGreen assay kit, respectively. The encapsulation efficiency (EE) of our LNPs, defined as the percentage of mKRAS entrapped inside the LNPs relative to total mRNA, demonstrated EE values of 92%. The corresponding EE value for cGAMP was 82%. The stability of the cGAMP/mKRAS/LNP formulation was confirmed by monitoring size and EE continuously at 4 °C for 15 days. The results showed a 10% increase in size (Figure 2D), with a minimal impact on EE (Figure 2E). Similar stability results were obtained when the cGAMP/mKRAS/

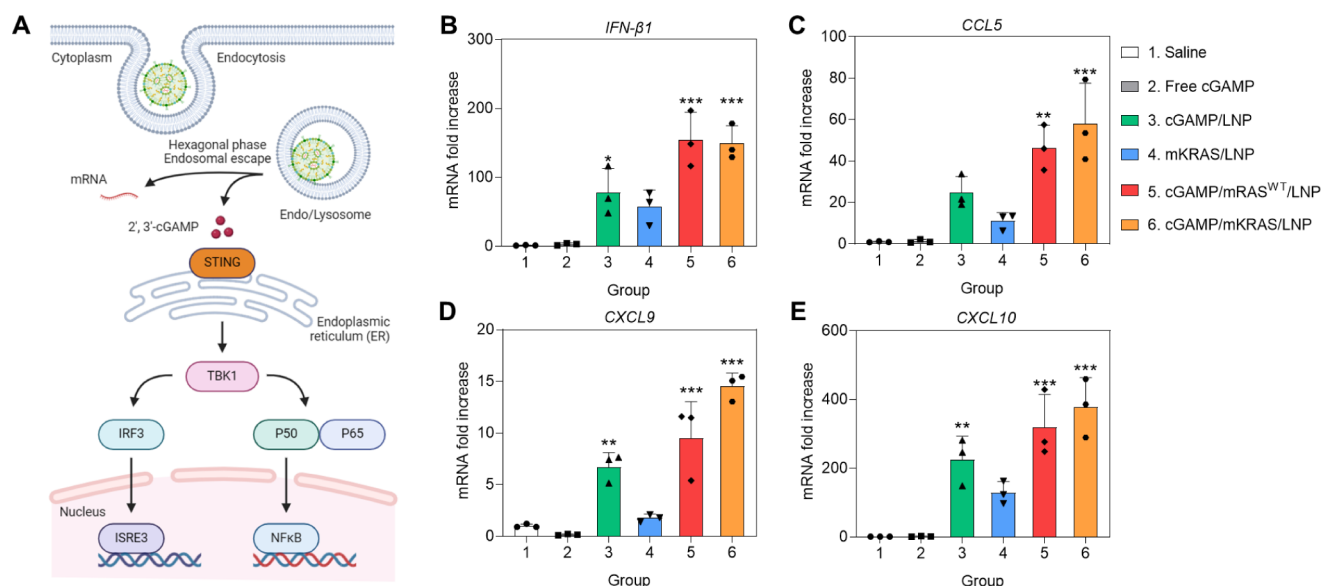


**Figure 3.** Activation of the cellular STING pathway by encapsulated cGAMP. (A) Intracellular delivery of 2'3'-cGAMP using LNP technology. Cytosolic 2'3'-cGAMP serves as a messenger for activating STING. STING activation triggers the TBK1/interferon regulatory factor 3 (IRF3) and NF- $\kappa$ B pathways, leading to transcriptional activation of type I IFNs and other pro-inflammatory cytokines.<sup>21</sup> (B–E) BMDCs were incubated with saline, free cGAMP, cGAMP/LNP, mKRAS/LNP, cGAMP/mKRAS<sup>WT</sup>/LNP, and cGAMP/mKRAS/LNP for 24 h, delivering cGAMP and mRNA at concentrations of 1  $\mu$ g/mL and 4  $\mu$ g/mL, respectively. Following cellular extraction and preparation of cDNA, RT-PCR was performed to establish the fold increase in the activation and expression of IFN- $\beta$ 1 mRNA (B), CCL5 mRNA (C), CXCL9 mRNA (D), and CXCL10 mRNA (E). \*  $p < 0.05$ , \*\*  $p < 0.01$ , \*\*\*  $p < 0.001$ .

LNP was incubated in PBS containing 10% FBS, or RPMI 1640 culture medium, supplemented with 10% FBS (Figure S3).

The intracellular release of mRNA from the LNP is dependent on the ionizable lipid component forming a hexagonal lipid phase for fusion with the APC endosomal membrane. The acidic microenvironment within endosomes and lysosomes is responsible for a charge reversal in the MC3 lipid, which transitions from a neutral state to a positively charged state. This charge alteration facilitates electrostatic interactions promoting membrane fusion between the LNPs and the endosomal/lysosomal membrane, allowing for intracellular release of the mRNA strand and cGAMP. To evaluate the preservation of this mechanism in the presence of cGAMP, we conducted red blood cell (RBC) lysis as a surrogate membrane for assessing the hexagonal phase. RBCs were suspended in PBS at pH 7.4 or 5.5, before incubation with cGAMP/mKRAS/LNP or mKRAS/LNP at concentrations of 0.5  $\mu$ g/mL, 1  $\mu$ g/mL, and 2  $\mu$ g/mL. Triton X-100 was used as a positive control for total RBC lysis. As shown in Figure S4A, both particle types induced concentration-dependent RBC lysis at pH 5.5, while no lysis occurred at pH 7.4. Figure S4B details the percent hemolysis compared to Triton (100%). These results demonstrate that cGAMP encapsulation does not impact the generation of the hexagonal phase, safeguarding effective release of mRNA and dinucleotide from the LNP.

**Activation of the STING Pathway by Encapsulated cGAMP.** The cGAS-STING signaling pathway, comprised of cyclic GMP-AMP synthase (cGAS) and the transmembrane protein STING, inserted in the endoplasmic reticulum membrane, plus downstream signaling adapters, plays a crucial role in protective immune defense against microbial infections or internal damage-associated DNA (Figure 3A).<sup>22,23,28,29</sup> cGAMP effectively activates the STING pathway and its downstream signaling cascades, including TBK1-IRF3 and NF-

$\kappa$ B, leading to the induction of type I IFNs, such as IFN- $\beta$ , and pro-inflammatory cytokines like IFN- $\gamma$ , thereby enhancing immune responses within the tumor microenvironment.<sup>22,23,28,29</sup> There is significant therapeutic interest in the use of STING agonists for cancer immunotherapy, with nanoparticles presenting a promising approach,<sup>15,16,23,30,31</sup> This includes the role of nanoparticles, capable of overcoming the negative charge of dinucleotides that prevent membrane permeation, as well as protecting the cargo to allow liver uptake. The endocytic uptake mechanism of LNPs by APC in the liver is predominantly mediated by a clathrin-mediated pathway.<sup>32</sup>

To investigate whether encapsulated cGAMP could activate the STING pathway, we examined the *in vitro* induction of STING-pathway relevant interferon  $\beta$ -1 (IFN- $\beta$ 1), CCL5, CXCL9, and CXCL10 mRNA expression, using RT-PCR. This analysis reflects the robust impact of the STING pathway on IFN- $\beta$ 1 and related cytokine/chemokine production in the liver, capable of activating immune responses that combat viral infections and the elimination of infected cells.<sup>33</sup> Similarly, CCL5, CXCL9, and CXCL10 are chemokines involved in the recruitment and activation of innate and adaptive immune responses, playing key roles in inflammation and immune surveillance.<sup>34,35</sup> RT-PCR expression analysis was conducted in bone marrow-derived DC cells (BMDC). Using a series of primers to quantify mRNA expression of IFN- $\beta$ 1, CCL5, CXCL9, and CXCL10, we observed the respective mRNA levels increasing by 149, 58, 15, and 378-fold during cGAMP/mKRAS/LNP treatment compared to the untreated control (Figure 3B–E). Similar increases were also observed in cells treated with cGAMP/LNP or cGAMP/mKRAS<sup>WT</sup>/LNP, while treatment with free cGAMP or mKRAS/LNP failed to show significant increases in mRNA expression. The small responses generated by mKRAS alone are likely due to the release of the nucleic acid strand that triggers the STING pathway

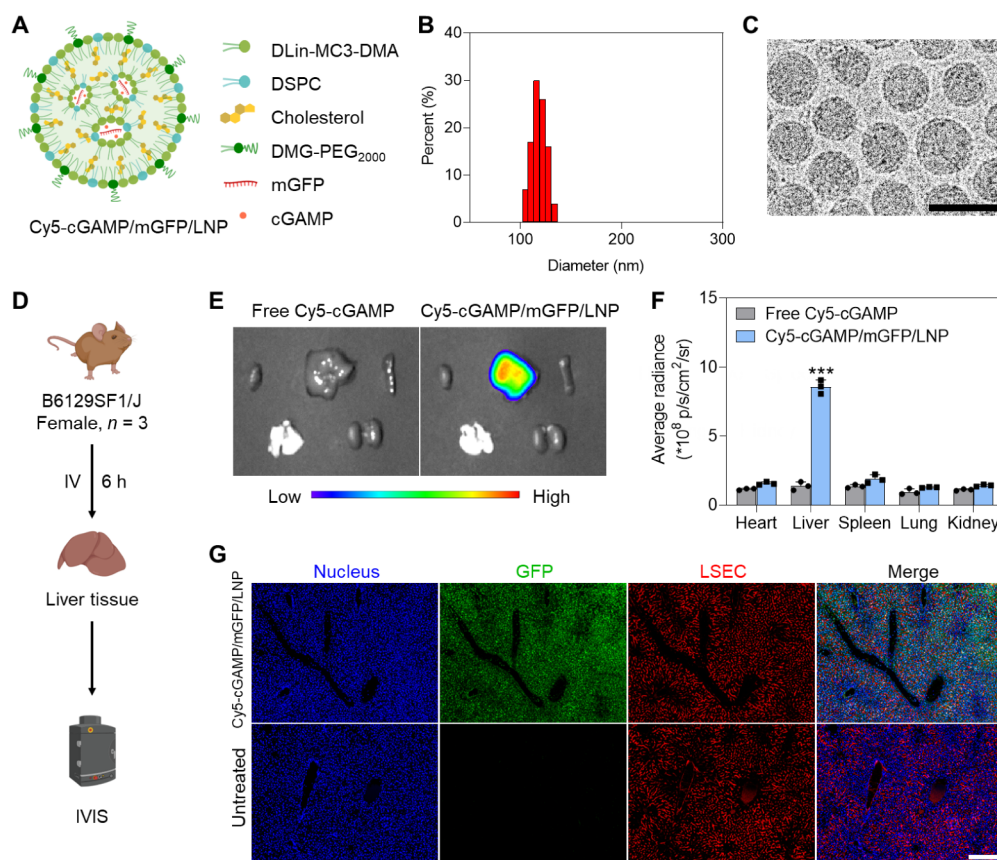


**Figure 4.** Biodistribution and *in vivo* mRNA translation of cGAMP/mGFP/LNP. (A) Fluorescent labeled Cy5-cGAMP as well as mGFP were used for the synthesis of Cy5-cGAMP/mGFP/LNP to determine LNP distribution, liver uptake, and mRNA expression after IV injection. (B) Size distribution of Cy5-cGAMP/mGFP/LNP (C) Representative cryoEM images of Cy5-cGAMP/mGFP/LNP. Scale bar is 100 nm. (D) The experimental planning involved IV injection into female B6129SF1/J mice for *in vivo* IVIS imaging, followed by animal sacrifice and harvesting the major organs (heart, liver, spleen, lung, and kidneys) for *ex vivo* IVIS imaging. (E) Representative *ex vivo* images of main organs from mice injected with Cy5-cGAMP/mGFP/LNP. The signals are from the Cy5 Ex/Em wavelength. (F) Average radiance efficiency of Cy5 from main organs. (G) Immunofluorescence staining of liver tissue slides. Nuclear, GFP, and LSEC staining were performed with DAPI, anti-GFP antibody, and anti-CD146 antibody, respectively. The colocalization index of GFP in relation to LSECs was assessed by image J analysis, amounting to  $12.3\% \pm 1.4\%$ . Scale bar is 200  $\mu\text{m}$ . \*\*\*  $p < 0.001$ .

intracellularly. These data confirm that encapsulated cGAMP effectively stimulates the STING pathway. This experiment was repeated in KPC cells, which were generated from the transgenic KrasLSL G12D+/Trp53LSL R172H+/Pdx-1-Cre mouse model. The RT-PCR results demonstrate increases of 201, 94, 22, and 43-fold in the expression of *IFN- $\beta$ 1*, *CCL5*, *CXCL9*, and *CXCL10* mRNA, respectively, during treatment with cGAMP/mKRAS/LNP (Figure S5A–D). No response was seen for mKRAS alone.

To determine the impact of cGAMP/mKRAS/LNP on DC maturation, we monitored the surface expression of CD80 and CD86 in murine BMDCs. CD80 and CD86 are crucial costimulatory molecules on these APCs that interact with CD28 on T cells, providing “signal 2”, as depicted in Figure S6A.<sup>36</sup> Exposure of DCs to cGAMP/LNP, cGAMP/mRAS<sup>WT</sup>/LNP, and cGAMP/mKRAS/LNP significantly increased the percentage of CD80<sup>+</sup>/CD86<sup>+</sup> cells from 32% in the saline group to 62%, 57%, and 63%, respectively (Figure S6B–D). In contrast, mKRAS/LNP alone was ineffective. Lipopolysaccharide (LPS) treatment served as a positive control. These results confirm that encapsulated cGAMP effectively promotes DC maturation.

**Encapsulated cGAMP Reprograms Liver APC Maturation Markers and is Accompanied by Generation of**

**IFN- $\gamma$  Producing Effector and Memory T Cells.** To demonstrate the effective delivery of cGAMP for reprogramming costimulatory receptor expression in liver NPC populations, including LSECs, Kupffer cells, and DCs, LNP carriers were developed for Cy5-labeled cGAMP as well as an mRNA strand encoding green fluorescent protein (mGFP) expression (Figure 4). This required the creation of Cy5-cGAMP/mGFP/LNP using a microfluidics approach for which the components are shown in Figure 4A. The resulting Cy5-cGAMP/mGFP/LNP had a size of 132 nm, with the accompanying cryoEM features illustrated in Figure 4B,C. These particles were IV injected, followed by harvesting of major organs (including the heart, liver, spleen, lungs, and kidneys) 6 h later for *ex vivo* IVIS imaging (Figure 4D). The Cy5 signal was exclusively discernible in the liver of animals receiving encapsulated but not free Cy5-cGAMP (Figure 4E). Quantitative analysis of the Cy5 radiance is shown in Figure 4F. No significant uptake of encapsulated particles was seen in other organs. Furthermore, harvested liver tissues were sectioned and subjected to immunofluorescence microscopy, which showed GFP expression throughout the liver, including uptake by red fluorescent-labeled LSECs (Figure 4G). The slides from untreated mice were used as a negative control. The average colocalization rate of GFP (green channel) and

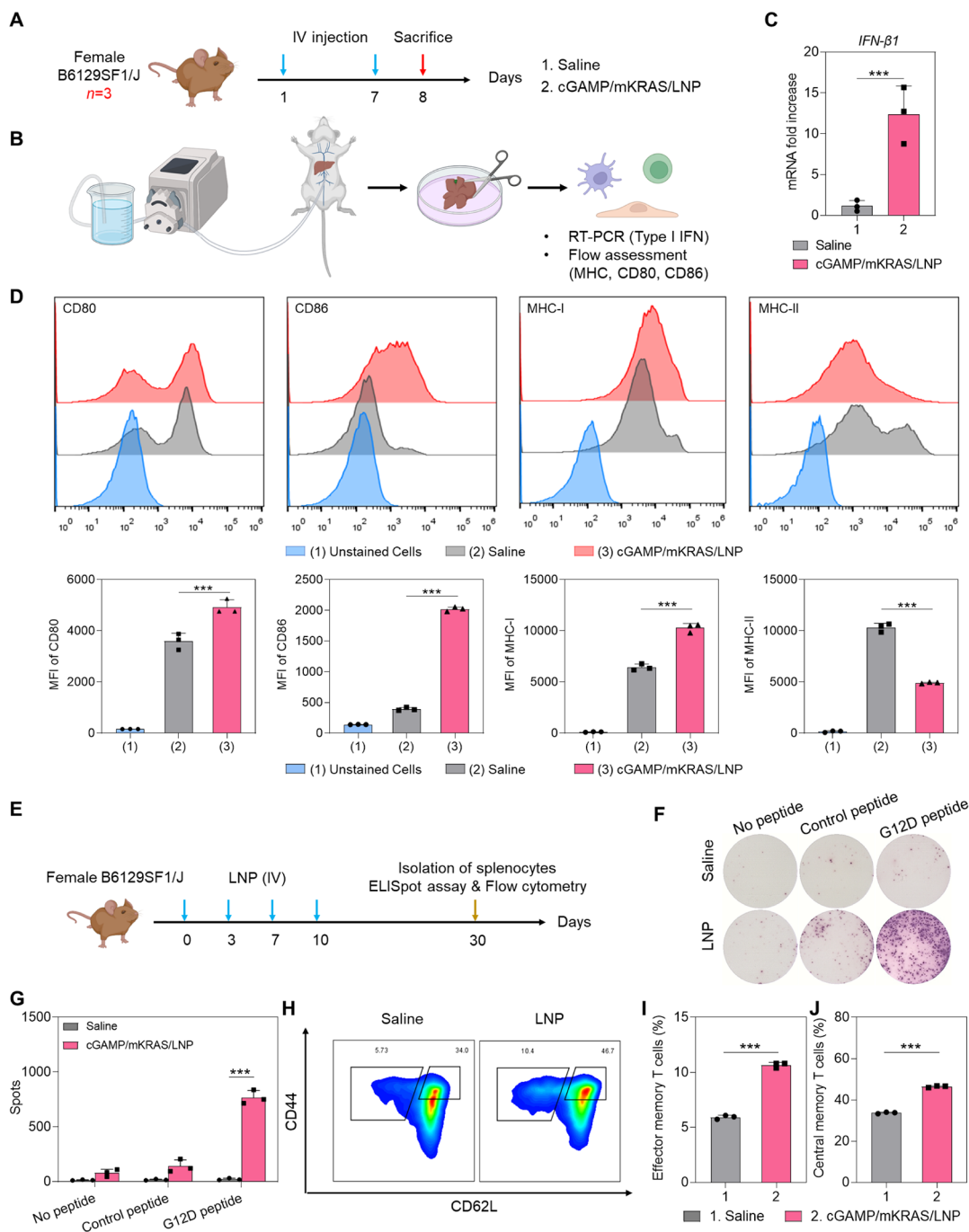


**Figure 5.** The immune reprogramming of liver NPCs and activation of cytotoxic and memory T cells by LNPs. (A) Experimental design to study the effect of cGAMP/mKRAS/LNP in NPCs. Briefly, two particle doses (0.3 mg/kg cGAMP and 1.25 mg/kg mKRAS each) were IV injected in female B6129SF1/J mice on days 1 and 7. (B) NPCs were extracted from *in vivo* perfused liver tissues (collagenase buffer) before animal sacrifice and harvesting, with NPCs used for RT-PCR and flow cytometry. (C) RT-PCR to assess the fold increase in *IFN-β1* mRNA expression, following treatment with saline or cGAMP/mKRAS/LNP ( $n = 3$ ). (D) Representative plot to display fluorescence intensity distribution as well as statistical histograms for CD80, CD86, MHC-I, and MHC-II expression in NPCs. (E) Schematic to describe the *in vivo* assessment of immune activation parameters in mice receiving IV injection of 4 doses of saline or cGAMP/mKRAS/LNP. Animals were sacrificed to separate splenocytes for ELISPOT assays and flow cytometry. (F) ELISPOT assays were conducted by treating the splenocytes with the G12D or wild-type peptide for 24 h and assessing *IFN-γ* producing colonies. (G) Quantitative analysis of ELISPOT colonies ( $n = 3$ ). (H) Flow cytometry to assess CD44 and CD62L expression in CD3<sup>+</sup>/CD8<sup>+</sup> splenocytes. CD44<sup>+</sup>CD62L<sup>+</sup> T cells represent central memory T cells, while CD44<sup>+</sup>CD62L<sup>-</sup> cells are considered as effector memory T cells. (I and J) Statistical expression of the percentage of effector memory and central memory T cells ( $n = 3$ ). \*\*\*  $p < 0.001$ .

LSECs (red channel) in our experiment was  $12.3\% \pm 1.4\%$ , as quantified using ImageJ software. Additionally, Mander's coefficients were calculated with ImageJ, yielding a value of  $0.13 \pm 0.012$ . This is compatible with the demonstration that

ionizable LNPs target multiple liver cell types, including hepatocytes and NPCs.<sup>27</sup> LSECs and Kupffer cells represent two of the principal tolerogenic APC types in the liver,

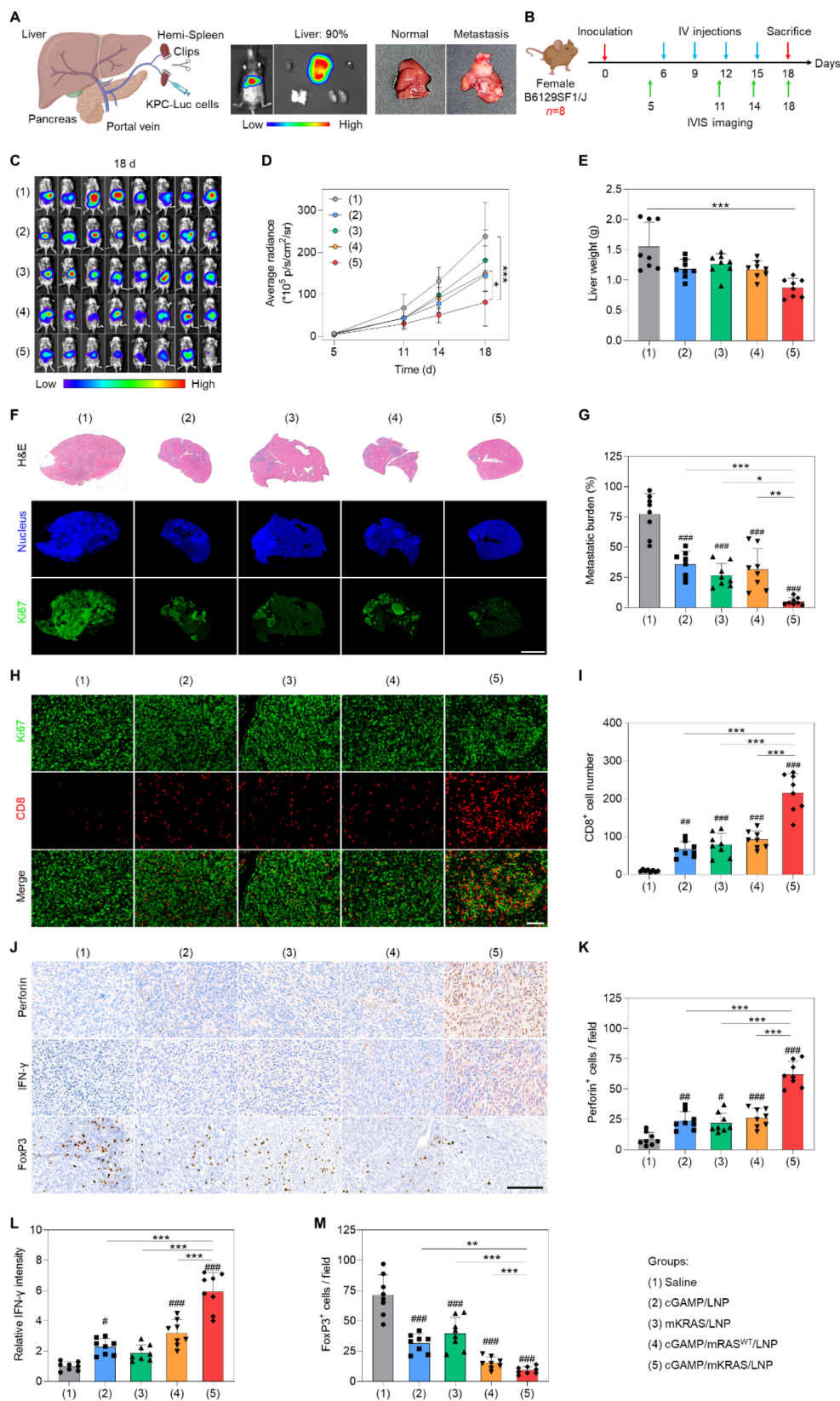


**Figure 6.** *In vivo* therapeutic effect of KRAS mutant epitope mRNA delivering LNP against PDAC liver metastasis. (A) Diagram to explain hemispleen injection of KPC-luc cells to obtain liver metastases. IVIS images taken *in vivo* on day 14 after tumor inoculation show the signal from the KPC-luc cells in the liver. The photograph demonstrates the appearance of a liver with metastases. (B) Schematic describing the investigation of the therapeutic effect in mice receiving IV injection of 4 doses of saline or cGAMP/LNP, mKRAS/LNP, cGAMP/mRAS<sup>WT</sup>/LNP, or cGAMP/mKRAS/LNP (0.3 mg/kg cGAMP and 1.25 mg/kg mKRAS or mRAS<sup>WT</sup>). Tumor growth was monitored by IVIS imaging and body weight was recorded every 3 days. All mice were sacrificed on day 18 for the collection of blood and liver tissues. (C) *In vivo* IVIS images of the animals on day 18. (D) Summary of average radiance from the liver area for each group ( $n = 8$ ). (E) Liver weights on day 18.

Figure 6. continued

(F) Representative H&E images and fluorescence images of the liver slices in each group. Scale bar is 5 mm. (G) Statistical analysis of metastatic burden from each H&E image ( $n = 8$ ). (H) Representative fluorescence images for Ki67 and CD8 staining in liver slides. (Scale bar is 100  $\mu\text{m}$ ) (I) Statistical analysis of the number of CD8<sup>+</sup> T cells representative of each group ( $n = 8$ ). (J) IHC staining for perforin, IFN- $\gamma$ , and FoxP3. The scale bar is 50  $\mu\text{m}$ . (K) Statistical analysis of the number of Perforin<sup>+</sup> cells in each group in the IHC stained images ( $n = 8$ ). (L) Statistical analysis of IFN- $\gamma$  intensity for each group in the IHC stained images ( $n = 8$ ). (M) Statistical analysis of FoxP3<sup>+</sup> cell number in each group in the IHC stained images ( $n = 8$ ). \* $p < 0.05$ , \*\* $p < 0.01$ , \*\*\* $p < 0.001$ , # $p < 0.05$ , ## $p < 0.01$ , ### $p < 0.001$ .

contributing to the tolerance and immune protection against cancer.<sup>37</sup>

To determine whether cationic LNP containing cGAMP and mKRAS mRNA (cGAMP/mKRAS/LNP) can reprogram antigen-presenting cells (APCs) in the liver to boost the cytotoxic T cell response, we assessed the effects on the nonparenchymal cell (NPC) fraction, including the hepatic APCs. Mice were treated with cGAMP/mKRAS/LNP on days 1 and 7, followed by *in vivo* liver perfusion under anesthesia. This allows proper tissue dissociation using a collagenase IV buffer that enzymatically digests the liver and allows density separation of the NPC fraction (Figure 5A). Due to the limitation of the number of mice that can be kept under anesthesia at one time, the performance of comparative analysis of other LNP compositions was carried out in separate experiments in tumor-bearing mice. The NPC cell suspension was used to evaluate IFN- $\beta$ 1 mRNA expression in LNP vs saline-treated animal livers, using RT-PCR, as well as assessing costimulatory receptor (CD80, CD86, MHC-I, and MHC-II) expression, carried out by a standardized flow cytometry procedure as outlined in the Methods section (Figure 5B).

RT-PCR analysis revealed a 12.5-fold increase in IFN- $\beta$ 1 mRNA expression following cGAMP/mKRAS/LNP treatment (Figure 5C), indicating an increased expression of a major STING pathway transcriptional activation event *in vivo*. Flow cytometry further demonstrated upregulation of the CD80, CD86, and MHC-I expression on NPCs, confirming the attainment of a KPC phenotype that induces cytotoxic T cell activation (Figures 5D and S7). This includes MHC-I expression for presenting the KRAS epitopes to cytotoxic T cells in generating an antitumor immune response.<sup>38</sup> Conversely, MHC-II expression, which is associated with tolerogenic antigen presentation to regulatory T cells (Tregs), was downregulated.<sup>6,38</sup> These phenotypic changes show that the cGAMP/mKRAS/LNP is capable of promoting a KRAS-mediated immune response by improving MHC-I antigen presentation, with the assistance of costimulatory signal delivery by CD80 and CD86, as previously established.<sup>40</sup>

To further evaluate whether cGAMP/mKRAS/LNP induces a robust IFN- $\gamma$  producing T cell response, female B6129SF1/J mice ( $n = 3$ ) received 4 intravenous administrations of either saline or the nanoparticle formulation. After 20 days, the mice were sacrificed and splenocytes were harvested for IFN- $\gamma$  ELISPOT assays (Figure 5E). Splenocytes from saline-treated mice showed minimal cytokine spots when stimulated with either G12D or wild-type peptides. In contrast, cGAMP/mKRAS/LNP-treated mice showed a significant increase in IFN- $\gamma$ -producing spots in response to the G12D peptide, but not the wild-type peptide (Figure 5F,G). This indicates specificity of the immune response to the mutant KRAS analog.

To further assess the contribution of memory T cells to the response, flow cytometry was performed on harvested

splenocytes as described in the Methods section. This involved analyzing the abundance of CD44<sup>+</sup>CD62L<sup>+</sup> (central memory, TCM) and CD44<sup>+</sup>CD62L<sup>-</sup> (effector memory, TEM) subsets within the CD3<sup>+</sup>/CD8<sup>+</sup> gated population. Memory T cells, which differentiate from effector T cells (Figure S8A), play a critical role in long-term immune surveillance.<sup>41</sup> Both TCM and TEM populations were significantly expanded in cGAMP/mKRAS/LNP-treated mice (Figures 5H–J and S8B), demonstrating the presence of cells that can initiate a secondary antigen-specific immune response. This finding highlights the feasibility of using this approach for adoptive transfer experiments, as discussed later.<sup>42</sup>

**Use of a KPC Metastasis Model to Demonstrate the Therapeutic Efficacy of cGAMP/mKRAS/LNP.** A PDAC metastasis mouse model was established using hemispleen injection of KPC-luc cells, as detailed in Figure 6A.<sup>39</sup> IVIS imaging confirmed that the KPC-luc cells are retained in the liver, without impacting the heart, lungs, kidneys, or the remaining portion of the spleen. This liver-specific growth was further corroborated by photographing the harvested liver tissues. While establishing this model, the number of injected KPC-luc cells was also adjusted to align the tumor burden with the duration of animal survival, with 50,000 cells resulting in animal demise within 16–22 days, while injecting 10,000 cells led to fatality within 26–32 days.

To assess the therapeutic impact of cGAMP/mKRAS/LNP in a PDAC metastasis model, animals injected with  $5 \times 10^4$  KPC-luc cells on day 0 received four IV injections of cGAMP/LNP, mKRAS/LNP, cGAMP/mKRAS<sup>WT</sup>/LNP, or cGAMP/mKRAS/LNP on days 6, 9, 12, and 15 (Figure 6B). Each injection delivered a cGAMP dose of 0.3 mg/kg or an mRNA dose of 1.25 mg/kg. Tumor growth was monitored by IVIS imaging, showing visible tumor growth on day 5, evolving to strong radiance on day 18 (Figures 6C and S9A). Among the treated groups, mice receiving cGAMP/mKRAS/LNP showed the least increase in radiance intensity, demonstrating robust statistical deviation from animals treated with saline ( $p < 0.001$ ), cGAMP/LNP ( $p < 0.05$ ), mKRAS/LNP ( $p < 0.05$ ), or cGAMP/mKRAS<sup>WT</sup>/LNP ( $p < 0.05$ ) (Figure 6D). Body weight was recorded every 3 days (Figure S9B), and liver weight was measured at the time of animal sacrifice. This showed a lesser liver weight gain in the dual cGAMP and mKRAS treatment group (Figure 6E). This is consistent with quantification of luciferase radiance during *ex vivo* IVIS imaging (Figure S9C), which showed a strong statistical deviation ( $p < 0.001$ ) for cGAMP/mKRAS/LNP versus saline, with lesser impact ( $p < 0.05$ ) by other treatment groups (Figure S9D). These results suggest that cGAMP/mKRAS/LNP can effectively interfere with metastatic growth.

To further evaluate the immune response in the metastatic liver model, histology and immunohistochemistry were used to compare H&E with fluorescence staining, involving DAPI staining to detect nuclei (purple blue) and Ki67 fluorescence (green) for assessing cellular proliferation. Collectively, these

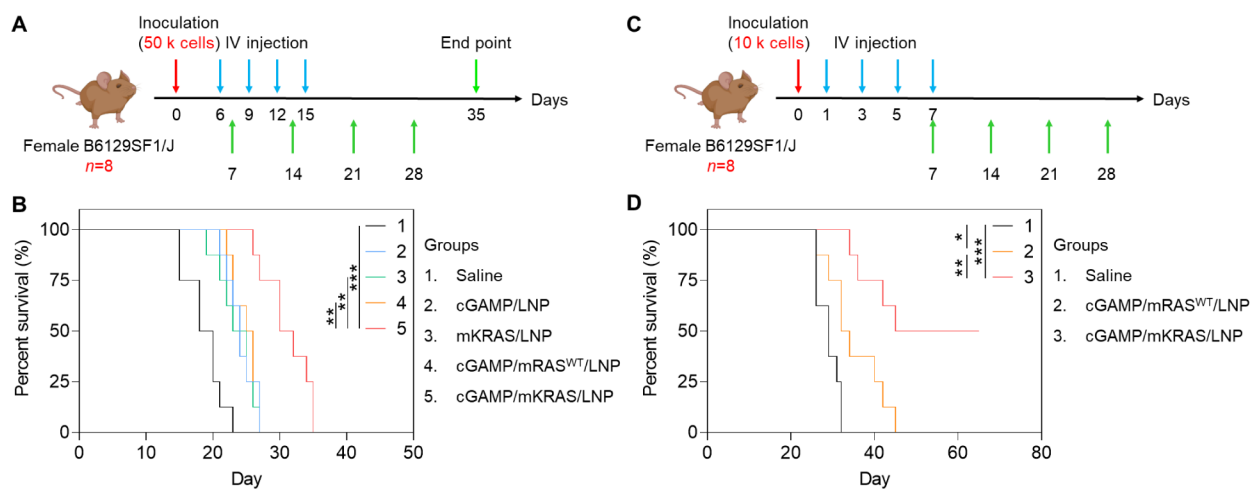


**Figure 7.** Survival in the post-treatment model. (A) Schematic of the survival study in mice receiving  $5 \times 10^4$  KPC-luc cells by hemispleen injection. Four doses of cGAMP/LNP, mKRAS/LNP, cGAMP/mRAS<sup>WT</sup>/LNP, or cGAMP/mKRAS/LNP (0.3 mg/kg cGAMP and 1.25 mg/kg mKRAS or mRAS<sup>WT</sup>) were IV injected on days 6, 9, 12, and 15. Tumor growth was monitored by IVIS imaging every week. (B) Survival plots of the different groups ( $n = 8$ ). (C) Schematic of similar survival study, where the animals received 4 doses of cGAMP/mRAS<sup>WT</sup>/LNP or cGAMP/mKRAS/LNP on days 1, 3, 5, and 7, before hemispleen injection with  $1 \times 10^4$  KPC-luc cells. Because of the similarity between groups 2–4 in panel B, cGAMP and mKRAS were not included for logistical reasons in this experiment. Tumor growth was monitored by IVIS imaging every week. (D) Survival plot of different groups ( $n = 8$ ). \* $p < 0.05$ , \*\* $p < 0.01$ , \*\*\* $p < 0.001$ .

results showed a significant effect on KPC metastatic growth in the liver during LNP treatment (Figure 6F). Accompanying H&E staining demonstrated noticeable shrinkage of the nuclear-dense area (corresponding to the Ki-67-stained loci) in response to treatment, particularly prominent in the cGAMP/mKRAS/LNP group. These images were used for calculating the metastatic burden, defined as the area occupied by metastatic foci relative to the total liver surface area (Figure 6G). The average metastatic burden in the cGAMP/mKRAS/LNP group was 6%, which was significantly lower than in the other groups. This demonstrates the superior antitumor effect of cGAMP/mKRAS/LNP treatment. Quantification of serum IL-6 and IL-10 (Figure S9E,F) was carried out to assess whether the encapsulation of the STING agonist leads to systemic cytokine release, capable of generating a cytokine storm during systemic administration of nonencapsulated STING agonists.<sup>40</sup> No increase in the levels of the cytokines was demonstrated, which is in keeping with improved safety by encapsulating the STING agonist in a nanocarrier. It is also worth mentioning that due to the transient kinetics of STING pathway activation by nanoparticles, usually in the range of 24–48 h,<sup>41</sup> we did not assess IFN- $\beta$ 1 production at the metastatic PDAC site, where organ harvesting occurred 72 h after the last injection of cGAMP/mKRAS/LNP (Figure 6B), compared to 24 h in Figure 5.

To relate the decline in metastatic burden to antitumor immunity, immunohistochemistry was performed to assess CD8<sup>+</sup> T cell recruitment to the Ki-67-rich tumor loci (Figure 6H). While a paucity of T-cells was observed in the saline-treated group, a significant increase in the level of CD8<sup>+</sup> T cell recruitment was observed in the other treatment groups. The most substantial increase was for the cGAMP/mKRAS/LNP-treated group, showing CD8<sup>+</sup> T cell levels were 25 times higher than those of the saline group, while also deviating statistically from other treatment groups (Figure 6I). The increased number of cytotoxic T cells was also accompanied by perforin deposition and IFN- $\gamma$  immunohistochemistry staining, as demonstrated in Figure 6. To assess whether these immune

stimulatory effects were accompanied by a change in the number and spatial distribution of immune suppressive cells in the tumor microenvironment, immunohistochemistry staining was performed for Treg (FoxP3) and M2 macrophage (CD163) biomarkers<sup>42</sup> (Figures 6J–M and S10). The significant reduction in FoxP3<sup>+</sup> Tregs in the tumor microenvironment of the cGAMP/mKRAS/LNP-treated group confirmed the decrease in this immune suppressive population. We also assessed M2 macrophage expression by CD163 staining but could not observe the presence of a significant cell number in the tumor microenvironment (Figure S10).

**Survival Impact of cGAMP/mKRAS/LNP as a Therapeutic Response Model.** To determine the survival impact of cGAMP/mKRAS/LNP administration in mice injected with  $5 \times 10^4$  KPC-luc cells, a similar experiment was performed to compare the administration of treatment on days 6, 9, 12, and 15 (Figure 7A). Mice in the saline group had a median survival of 19 days (ranging from 15 to 23 days). In contrast, the median survival for animals receiving cGAMP/LNP, mKRAS/LNP, cGAMP/mRAS<sup>WT</sup>/LNP, and cGAMP/mKRAS/LNP was 24 days, 24 days, 25.5 days, and 31 days, respectively (Figures 7B and S11). The significant improvement in the median survival of the cGAMP/mKRAS/LNP group demonstrates the synergistic effect of cGAMP and mKRAS codelivery.

Subsequently, we studied the survival rate for mice receiving hemispleen injection of  $1 \times 10^4$  KPC-luc cells, followed by treatment with saline, cGAMP/mRAS<sup>WT</sup>/LNP, and cGAMP/mKRAS/LNP (Figure 7C). For logistical reasons and in accordance with the principle of “reduction in animal research”, encapsulated cGAMP only was omitted considering its lesser efficacy in the experiment described in Figure 6. The Kaplan–Meier plot indicates that while animals treated with saline had a median survival of 29 days, those treated with cGAMP/mRAS<sup>WT</sup>/LNP and cGAMP/mKRAS/LNP had median survival times of 33 days and 55 days, respectively (Figures 7D and S12). Noteworthy, 50% of the animals treated with cGAMP/mKRAS/LNP remained alive up to day 63, when the animals were sacrificed. This suggests the possibility

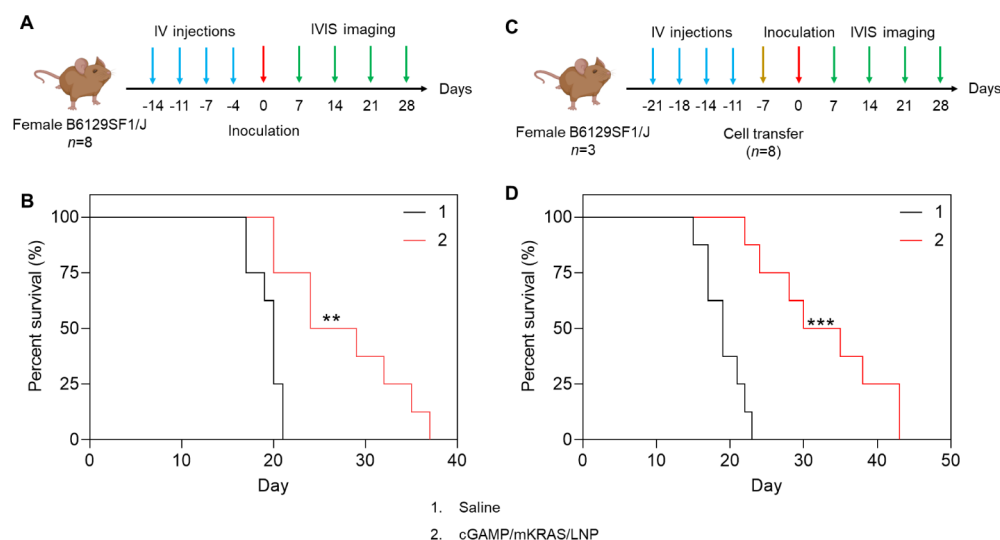


**Figure 8.** Impact of cGAMP/mKRAS/LNP in prophylactic treatment and adoptive cell transfer. (A) Schematic of the survival study of mice pretreated with different formulations, followed by inoculation with  $5 \times 10^4$  KPC-luc cells by hemispleen injection. Four doses of saline or cGAMP/mKRAS/LNP (0.3 mg/kg cGAMP and 1.25 mg/kg mKRAS) were IV injected on days -14, -11, -7, and -4. Tumor growth was monitored by IVIS imaging. (B) Survival plots for the two groups ( $n = 8$ ). For logistical reasons, the only comparison was to saline. (C) Schematic of the survival study in animals receiving adoptive transfer of splenocytes from vaccinated animals. Vaccinated animals received 4 doses of saline or cGAMP/mKRAS/LNP (similar amount of cargo as for A) on days -21, -18, -14, and -11, before euthanasia on day -7 to isolate lymphocytes from the spleen. The cells were used for adoptive transfer into healthy recipient animals ( $n = 8$ ), each receiving  $3 \times 10^6$  lymphocytes intravenously.  $5 \times 10^4$  KPC-luc cells were injected into the hemispleen of untreated recipient mice on day 0. Tumor growth was monitored by IVIS imaging. (D) Survival plots for the animal groups in the adoptive transfer experiment ( $n = 8$ ). \*\* $p < 0.01$ , \*\*\* $p < 0.001$ .

of obtaining long-term survival using the cGAMP/mKRAS/LNP.

**The Impact of Prophylactic cGAMP/mKRAS/LNP Administration, Including the Use of Splenocytes for Adoptive Transfer to Nontreated Recipients.** The development of liver metastases in PDAC is often fatal, irrespective of the treatment response at the primary cancer site.<sup>4</sup> We therefore asked whether prophylactic administration could be used as a form of vaccination to prevent KPC metastatic growth in the liver (Figure 8A). Animals received the same dose of cGAMP/mKRAS/LNP in four IV administrations before splenic injection of  $5 \times 10^4$  KPC-luc cells for a survival experiment (Figure 8A). The resulting Kaplan–Meier plot shows that, in comparison to the saline control group (20 days), animal survival was significantly ( $p < 0.01$ ) extended by prior cGAMP/mKRAS/LNP treatment (Figures 8B and S13).

The prophylactic model was subsequently used to determine whether the retrieval of T cells from the spleen of LNP-injected animals can be used for adoptive transfer prior to injecting untreated recipients with  $5 \times 10^4$  KPC-luc cells in the hemispleen compartment (Figure 8C). The results show that the median survival of mice receiving adoptive transfer of lymphocytes from cGAMP/mKRAS/LNP-treated animals was 32.5 days, which was significantly higher ( $p < 0.001$ ) than 19 days for animals receiving lymphocytes from saline-treated animals (Figures 8D and S14). This is in keeping with the generation of memory T cells.

**Biosafety Assessment.** While the therapeutic use of STING agonists holds great promise for cancer immunotherapy and infectious disease treatment, systemic administration can trigger significant off-target effects due to potent immune system activation.<sup>43</sup> This includes the possibility of cGAMP generating a cytokine storm, which stands to be lessened by encapsulated delivery.<sup>44</sup> To determine if the same holds true

for the ionizable LNP, we undertook a biosafety experiment to assess the impact on cytokine levels in the serum as well as the assessment of biomarkers that reflect liver and renal toxicity. Four IV injections of cGAMP/mKRAS/LNP, each delivering a cGAMP dose of 0.3 mg/kg and an mKRAS dose of 1.25 mg/kg, were administered before blood collection and recording animal weight, as shown in Figure S15A. Saline and free cGAMP were used as the controls. Noteworthy, no significant change in body weight or physical evidence of general health decline was observed during daily inspections over 24 days (Figure S15B).

Blood collected from the animals on days 2, 11, and 24 was used to study serum cytokine concentrations (IL-6 and TNF- $\alpha$ ) as well as biomarkers that reflect liver (ALT and AST) or kidney (BUN and creatinine) damage. No significant changes in IL-6, TNF- $\alpha$ , ALT, AST, BUN, or creatinine levels were observed (Figures S15C–H). These results demonstrate that four doses of cGAMP/mKRAS/LNP (0.3 mg/kg cGAMP and 1.25 mg/kg mKRAS) are safe. We also did not observe evidence of animal toxicity in the studies described in Figures 6–8.

## DISCUSSION

In our study, we combined a STING agonist with a KRAS mRNA vaccine to explore the potential to generate an effective immune response in the liver for hard-to-cure metastatic pancreatic cancer. We demonstrate reprogramming of the tolerogenic immune environment in the liver to generate an effective immune response against often-fatal PDAC metastatic disease. In fact, we could achieve a 50% survival rate in an animal experiment where a lower dose of KPC was used (Figure 7D). This was attained by developing a lipid nanocarrier that delivers mRNA encoding a KRAS G12D neoantigenic peptide along with cGAMP, a STING agonist. The LNPs were synthesized using a microfluidics process,

enabling the nanoprecipitation of mRNA and cGAMP by the ionizable lipid MC3, to yield a 90-nm LNP. These carriers successfully activated the type I interferon pathway, also enhancing effective particle uptake and triggering IFN- $\beta$ 1 expression in the liver. Moreover, this was accomplished by generating IFN- $\gamma$  producing T cells, which could be detected in the spleen using ELISPOT assays. Additionally, cGAMP/mKRAS/LNP induced costimulatory receptor expression (CD80 and CD86) on nonparenchymal liver APCs, promoting the generation of cytotoxic and memory T-cells capable of mounting an effective immune response against a metastatic KPC mouse model. The efficacy of this approach was demonstrated by IV administration of cGAMP/mKRAS/LNPs, both prophylactically and following the establishment of metastases. The immune response at the metastatic tumor site was characterized by the recruitment of CD8<sup>+</sup> cytotoxic T-cells, leading to tumor shrinkage and prolonged survival. Moreover, the immune response could be adoptively transferred by injecting splenocytes, which contain memory in addition to cytotoxic T cells, into the recipient animals.

The most impactful finding of this study is the demonstration of synergy between the KRAS mRNA and the STING agonist nanoparticle components in combating PDAC liver metastasis (Figures 6–8). The liver is home to unique APCs for preventing an excessive immune response to foreign antigens from the gut.<sup>45</sup> This tolerogenic immune environment also allows the liver to protect itself or cotransplanted organs against rejection, as well as hindering protective immune responses against metastatic cancer cells.<sup>4,46</sup> Among the many pathways used by the liver for exerting immune suppressive effects is the generation of Tregs by Kupffer cells and LSECs.<sup>47,48</sup> We demonstrate that it is possible to reprogram the tolerogenic APC effects, which are dependent on differences of their unique antigen and processing effects as well as the production of tolerogenic cytokines.<sup>6,49,50</sup> When intracellularly delivered, cGAMP increases IFN- $\beta$ 1 production as well as engaging in upregulation of costimulatory receptors (CD80 and CD86) and MHC-I expression on liver NPCs (Figure 5). These phenotypic changes are known to favor MHC-I presentation of mutant KRAS epitopes to cytotoxic T-cells,<sup>51</sup> which also receive a CD28 costimulatory signal from binding to more abundant expression of the APC surface receptors, CD80 and CD86.

The ability to accomplish both vaccination as well as an adjuvant delivery with a single nanocarrier is highly advantageous, particularly when accomplishable with scalable carrier technology, which also enables incorporation of an ionizable lipid to promote uptake in the liver through the assembly of a protein corona that binds to the apolipoprotein E (ApoE) receptor.<sup>27,52</sup> Several liver cell types are targeted by this corona, including hepatocytes and tolerogenic APCs, including LSECs.<sup>6,27</sup> This approach also allows efficient nanoprecipitation of the negatively charged dinucleotide and mRNA by the cationic, ionizable lipid, e.g., MC3. It is notable that the synergy between these components applies to prophylactic as well as already established metastasis models, allowing for a range of PDAC immunotherapy interventions (Figure 8). The first is the potential to use a vaccination approach to prevent new metastatic spread to the liver in recently diagnosed PDAC patients. This may help to strengthen the efforts of establishing therapeutic responses at the primary tumor site, more conducive to prolonging life in the absence of metastases. However, the demonstration of enhanced survival beyond the

establishment of metastases also shows potential to improve immunotherapy, which may benefit the primary pancreatic cancer site. We are currently investigating this possibility in a KRAS orthotopic model, allowing the development of spontaneous liver metastases from the primary cancer site. This could allow us to combine our LNP technology with the established use of lipid bilayer-coated mesoporous silica nanoparticles (a.k.a. the silicasome nanocarrier), used by us for the delivery of chemoimmunotherapy that generates immunogenic cell death (e.g., irinotecan).<sup>18</sup> Immunogenic cell death (ICD) releases multiple endogenous antigens, with the possibility of subsequently triggering integration of the immune response at the primary cancer site into the cancer immunity cycle, generating polyclonal immune responses that involve the spleen and regional lymph nodes.<sup>53</sup> Thus, combining a polyclonal ICD response with a strong vaccination response to a neoantigen could boost the anti-PDAC immune response. This could include the participation of tertiary lymphoid follicles that develop at the primary PDAC site in response to KRAS vaccination.<sup>54</sup>

The use of STING agonists for boosting the immune response against infectious disease agents has been widely studied as therapeutics for boosting the type I interferon pathway, with an impact on innate immunity, cytokines, and chemokines.<sup>14–16,23,29</sup> From a therapeutic perspective, it is also important to emphasize the role of encapsulated delivery in terms of the safety of STING agonists. Negatively charged cyclic dinucleotides (CDNs), such as cGAMP, can lead to widespread innate immune activation when systemically administered, including the potential to generate severe inflammatory responses, also referred to as a cytokine storm.<sup>44,55</sup> However, restricted delivery to the liver reduces the risk of systemic toxicity and also allows APC uptake and reprogramming of the antitumor immune response. In addition to the use of an ionizable lipid, diacyl lipids have been employed for cGAMP conjugation and incorporation into nanodiscs, capable of inducing robust antitumor immunity.<sup>26</sup>

In the realm of cancer immunotherapy, STING agonists codelivered with mRNA vaccines have proven particularly potent in stimulating APCs through the STING pathway, leading to enhanced antitumor immunity with minimal systemic inflammation.<sup>16</sup> A recent study also highlighted the use of STING agonists with mRNA in lymph node-targeted nanoparticles, showing robust tumor-specific immune responses and long-term memory in murine models.<sup>15</sup> Moderna's mRNA-5671 (V941) is another cancer vaccine candidate that targets a combination of KRAS mutations, including G12D, G12V, G13D, and G12C, and is currently being evaluated for various KRAS-expressing cancers such as PDAC, nonsmall cell lung cancer, and colorectal cancer.<sup>14</sup> This vaccine includes four common KRAS mutations that activate CTLs via APC-mediated antigen presentation, showing promise in several solid tumors. Unlike mRNA-5671, our cGAMP/mKRAS/LNP approach uniquely incorporates a STING agonist to stimulate the type I interferon pathway, potentially enhancing immune activation within the tumor microenvironment and addressing the unique challenges of pancreatic cancer metastasis. This approach has not been used in the Moderna vaccine, as far as we can ascertain. Another example exploited new cationic lipids that serve as STING agonists and further assembled into LNP for enhanced antitumor efficacy.<sup>16</sup> These findings underline the potential of combining mRNA vaccines with STING agonists for both

cancer and infectious diseases but also point to the importance of additional unique formulations for combining adjuvants with a vaccine component targeting the liver to enhance efficacy. A major advance in the current study lies in addressing specific mechanistic limitations found in earlier designs, such as mRNA translation efficiency, while advancing targeted immunomodulatory responses not yet fully explored in the existing literature.

Our study has limitations. A major constraint is the exclusive use of the KRAS G12D mutation, despite the oncogenic evolution of cancer involving several KRAS mutations that need to be considered.<sup>1,56</sup> This limitation can be addressed by gene sequencing to determine the range of KRAS mutants present in an individual patient, as well as by preemptively incorporating multiple KRAS epitopes to cover a range of possibilities. While this study demonstrates antigen-specific T-cell activation through IFN- $\gamma$  ELISPOT assays as well as cytotoxic T cell localization at the tumor site, direct detection of KRAS/MHC I complexes *in vivo*, e.g., KRAS G12D or G12V mutations, is challenging. Although studies on KRAS epitopes have confirmed specific TCR recognition by the KRAS-MHC I complex, tetramer-based or direct binding evidence in the current literature remains sparse, including for Moderna's KRAS-targeted mRNA studies. Future studies could explore emerging methods or reagents to improve detection in the same model.<sup>51,57</sup> Moreover, although our research focused on a specific PDAC model, the potential application of this delivery platform may also be worth exploring for other cancer types. Recent research efforts have focused on developing LNPs to improve nucleic acid delivery to a variety of organs, including the lung, spleen, and bone.<sup>58</sup> In addition to the liver, we are interested in targeting the spleen and regional lymph nodes, which play a crucial role in generating anti-PDAC immunity.<sup>59,60</sup> Targeting these areas could improve the recruitment of an increased number of activated T cells in the cancer immune cycle. Furthermore, we anticipate that neoepitope vaccines will enhance precision medicine and cancer immunotherapy for PDAC.<sup>61</sup> While this study primarily focuses on the reprogramming of liver NPCs and the early activation of immune responses, we acknowledge the importance of effector and memory T cell dynamics in evaluating the synergistic therapeutic potential of cGAMP/mKRAS/LNP. Our data suggest that the combination treatment effectively stimulates T cell activation, as evidenced by IFN- $\gamma$  production and changes in T cell markers (CD44/CD62L). Although the detailed profiling of central and effector memory T cells was not the central aim of this study, the observed immune responses lay the foundation for the further exploration of long-term T cell memory formation in the future. These findings highlight the potential of cGAMP/mKRAS/LNP to drive not only immediate immune activation but also durable immune memory, warranting further exploration in future work.

In summary, this study shows that reprogramming the immune-protective niche for metastatic pancreatic cancer can be achieved by delivering a STING agonist and mutant KRAS mRNA via ionizable LNPs, offering both prophylactic and therapeutic benefits.

## MATERIALS AND METHODS

**Materials.** The ionizable lipid, MC3, was purchased from MedKoo Biosciences, Inc. All other lipids, including DSPC, cholesterol, and DMG-PEG<sub>2000</sub>, were purchased from Avanti Polar Lipids, Inc. The

mRNA strands, described below, were synthesized by TriLink Biotechnologies, using a 5' Cap and 3' PolyA modifications for stabilization. DiR and the RiboGreen RNA Assay Kit were purchased from Thermo Fisher Scientific.

**Design of KRAS and Wild-Type RAS Nucleic Acid Constructs.** We chose the G12D mutation, corresponding to amino acids (aa) 5–21 in KRAS, to generate an anti-PDAC immune response by constructing an mRNA (mKRAS) strand that includes 5 epitope repeats (Figure 1). The epitopes were flanked by two natural amino acids on the 5' and 3' ends. As a control, five repeats of the corresponding wild-type RAS (aa 5–21) sequence plus flanking aa were included in the mRAS<sup>WT</sup> construct. Following the addition of start and stop codons, optimization of the codon sequence was performed using the GenScript optimization tool. These sequences were shared with TriLink Biotechnologies to construct mKRAS and mRAS<sup>WT</sup> strands, as demonstrated in Figure S1.

**Preparation and Characterization of LNPs.** A microfluidics approach was used to synthesize a series of particles incorporating individual or combinations of cGAMP, mKRAS, or mRAS<sup>WT</sup>. For the synthesis of cGAMP/mKRAS/LNP, cGAMP, and mKRAS were dissolved in 0.1 M NaAc (pH 4.0), serving as the aqueous phase, while the lipid components, MC3, DSPC, cholesterol, and DMG-PEG<sub>2000</sub> were dissolved in ethanol, used as the organic phase. The MC3 ionizable cationic lipid enables effective mRNA delivery to the liver by forming a protein corona with blood proteins, which facilitates uptake by liver cells via receptor-mediated endocytosis. The binding of ApoE to MC3 on the LNP surface plays a role in directing the particle to liver cells through low-density lipoprotein receptors.<sup>62</sup> Once internalized, the acidic environment of endosomes ionizes the lipid, disrupting the endosomal membrane and releasing mRNA into the cytoplasm for translation. While hepatocytes are a target for mRNA expression, Kupffer cells and LSECs also participate in particle uptake. The natural liver tropism of MC3-LNPs and their efficient intracellular release make them a powerful platform for mRNA-based therapies. The molar ratio of MC3, DSPC, cholesterol, and DMG-PEG<sub>2000</sub> was 50, 10, 38.5, and 1.5, while the N/P ratio was 4. The aqueous and organic phases were blended in a NanoAssemblr at a 3:1 volume ratio and a flow rate of 12 mL/min. More details about composition and NanoAssemblr settings appear in Figure S2. The nanoprecipitated cGAMP/mKRAS/LNP were purified by dialysis against PBS (pH 7.4) at 4 °C for 1 h, followed by pushing through a 0.2  $\mu$ m cutoff filter. The particle size, PDI, and surface charge were assessed in a ZetaPlus (Brookhaven) instrument. Particle morphology and size were also assessed by cryogenic electron microscopy (Cryo-EM, TF20 FEI Tecnai-G2). The particle EE for cGAMP and mRNA was determined by cGAMP ELISA (Thermo) and RiboGreen assay kits (Thermo), respectively. A similar approach was used for the synthesis of carriers that incorporate cGAMP only (cGAMP/LNP), mKRAS only (mKRAS/LNP), or a combination of cGAMP with mRAS<sup>WT</sup> (cGAMP/mRAS<sup>WT</sup>/LNP). To assess particle uptake and expression of mGFP in the liver, a particle batch was synthesized for which the cGAMP and mKRAS were replaced by Cy5-cGAMP and mGFP, respectively, yielding Cy5-cGAMP/mGFP/LNP. The *in vitro* stability of LNP was assessed by monitoring LNP size, PDI, and EE during storage for 15 days at 4 °C.

### Hemolysis Assay to Assess the Hexagonal LNP Lipid Phase.

A hemolysis assay was conducted to determine the efficacy of the cationic lipid component in disrupting the RBC bilayer. This assay serves as a surrogate for the disruption of the endosomal membrane under acidic conditions, leading to mRNA release in the cytoplasm for translation.<sup>62</sup> Briefly, purified murine RBCs suspended in PBS at pH 5.0 or 7.4 were mixed with mKRAS/LNP or cGAMP/mKRAS/LNP at concentrations of 0.5, 1.0, or 2.0  $\mu$ g/mL for 1 h at 37 °C. 0.1% Triton solution was used as a positive control for expressing 100% RBC lysis. After centrifugation (1000 rpm, 5 min), the sample plate was photographed, and absorbance of the supernatants was assessed at 540 nm in a microplate reader (Molecular Devices, SpectraMax MS).

**In Vitro Transcriptional Activation by cGAMP, a STING Agonist.** BMDC and KPC cells were exposed to free cGAMP,

cGAMP/LNP, mKRAS/LNP, cGAMP/mRAS<sup>WT</sup>/LNP, or cGAMP/mKRAS/LNP (1  $\mu$ g/mL cGAMP, 4  $\mu$ g/mL mRNA) for 24 h at 37 °C. Total RNA was extracted by the TRIzol reagent (Thermo) and quantified by a NanoDrop Microvolume Spectrophotometer (Thermo). It has been demonstrated previously that cGAMP effectively activates signaling pathways, such as TBK1-IRF3 and NF- $\kappa$ B, downstream of the STING pathway, leading to increased expression of type I IFNs, such as IFN- $\beta$ 1. The RNA was used for cDNA synthesis after diluting in water (1:5, 1:25, 1:125, 1:625, and 1:3125), mixed with SYBR green mix and a series of primer pairs for IFN- $\beta$ 1, CCL5, CXCL9, and CXCL10. RT-PCR analysis was performed in a ViiA 7 RT-PCR System. mRNA expression was expressed as a fold increase over the PBS-treated group.

**BMDC Maturation.** Bone marrow cells were isolated from the femur and tibia of 6-week-old female B6129SF1/J mice, followed by culture in RPMI 1640 medium (10% FBS), supplemented with GM-CSF (20 ng/mL) and IL-4 (10 ng/mL) for 6 days. BMDCs were then harvested and transferred to a new plate. The cells were treated with cGAMP/LNP, mKRAS/LNP, cGAMP/mRAS<sup>WT</sup>/LNP, or cGAMP/mKRAS/LNP (1  $\mu$ g/mL cGAMP, 4  $\mu$ g/mL mRNA) for 24 h at 37 °C. Cells treated with LPS (1  $\mu$ g/mL) served as a positive control. Cells were stained with an antibody mixture (anti-CD11c, anti-CD80, and anti-CD86), followed by flow cytometry (Thermo Attune NxT) to assess CD80 and CD86 expression on CD11c<sup>+</sup> cells. BMDCs were also used for transcriptional activation of IFN- $\beta$ 1, CCL5, CXCL9, and CXCL10.

**LNP Biodistribution.** Biodistribution was carried out in 8-week-old female B6129SF1/J mice, using 3 animals per group. Six hours after IV injection of free Cy5-cGAMP or Cy5-cGAMP/mGFP/LNP (0.125 mg/kg Cy5-cGAMP, 0.5 mg/kg mGFP), IVIS imaging was carried out in a PerkinElmer Lumina II. Animals were sacrificed for organ harvesting and *ex vivo* imaging. We also collected paraffin-embedded liver tissues for sectioning and staining with DAPI, anti-GFP antibody, and anti-CD146 antibody. The reason for using the GFP antibody rather than GFP fluorescence is due to fluorescence decay during embedding and slicing. The slides were scanned in a Vectra Polaris Quantitative Pathology Imaging System. For the colocalization analysis, we randomly selected three different fields from each slide and used the green (GFP) and red (LSECs) channels to assess the GFP expression in LSECs. ImageJ software was employed for colocalization analysis, calculated as the ratio of the colocalization rate between green and red fluorescent cells. We also calculated Mander's coefficients using the ImageJ software.

**Analysis of Costimulatory and MHC Expression on Liver NPCs.** Mice ( $n = 3$ ) were IV injected with two doses of PBS or cGAMP/mKRAS/LNP (0.3 mg/kg cGAMP and 1.25 mg/kg mRNA) on days 0 and 7, before being anesthetized for *in vivo* perfusion with a collagenase-containing buffer. Animals were subsequently sacrificed, and liver tissue was used for the isolation of NPCs. The animals were then euthanized, and their livers were harvested for nonparenchymal cell (NPC) isolation. To separate NPCs from hepatocytes, we mechanically disrupted the enzymatically digested liver tissues and filtered them through a cell strainer to remove debris. The suspension underwent differential centrifugation, allowing the larger and denser hepatocytes to be pelleted at a low speed, with the NPCs remaining in the supernatant. The NPC-enriched fraction was further purified using density gradient centrifugation to enhance APC recovery, followed by washing and resuspension in appropriate media for downstream analyses. The NPC suspension was stained with a previously validated antibody panel that targets CD80, CD86, MHC-I, and MHC-II for flow cytometry analysis. The procedure is carried out according to a standardized protocol, commencing with viability assessment before cellular staining with the antibodies that were introduced, using the CD16/32 antibody first, before the addition of a combination of antibodies binding to CD80, CD86, MHC-I, and MHC-II. The procedure also includes fluorescence-minus-one controls for precise definition of gating and the use of positive controls.

**IFN- $\gamma$  ELISPOT Assay and Assessment of Memory T Cells.** Eight-week-old female B6129SF1/J mice were randomly assigned to 2

groups, each including three animals. Four doses of PBS or cGAMP/mKRAS/LNP (0.3 mg/kg cGAMP and 1.25 mg/kg mRNA) were IV injected every 3 days. Following animal sacrifice 20 days after the last injection, the spleens were harvested to isolate splenocytes. The cells were transferred into an ELISPOT plate and incubated in the presence of wild-type KRAS peptide ([Acetyl]-KLVVVGAGGVGKSALTI[Amide]) or KRAS G12D peptide ([Acetyl]-KLVVVGADGVGKSALTI[Amide]) for 24 h. The plate was washed and incubated with the BCIP/NBT substrate for 5–15 min to obtain the desired color intensity. After drying, the plate was imaged in an ELISPOT reader (CTL ImmunoSpot) to obtain the number of cytokine-producing spots using the instrument software.

To assess the presence of memory T cells, including for adoptive transfer, the same animal exposure conditions were used, followed by animal sacrifice 20 days after the last injection. Following euthanasia, spleens were harvested and processed into single-cell suspensions by mechanical disruption through a 70- $\mu$ m cell strainer. Red blood cells were lysed using an ammonium chloride-based lysis buffer, and the remaining leukocytes were washed and resuspended in flow cytometry staining buffer (PBS with 2% FBS). Splenocytes were incubated with a viability dye to exclude dead cells and anti-CD16/CD32 Fc block to minimize nonspecific binding. This was followed by staining with a fluorescently labeled antibody panel, including anti-CD3, anti-CD8, anti-CD44, and anti-CD62L. Cells were stained at 4 °C for 30 min in the dark, washed, and resuspended in buffer before analysis on an Attune NxT Flow Cytometer. Following the identification of single cells, gating was performed for the CD3<sup>+</sup>/CD8<sup>+</sup> subset before cross-gating on CD44 and CD62 to assess the presence of CD44<sup>+</sup>CD62L<sup>+</sup> (central memory) and CD44<sup>+</sup>CD62L<sup>-</sup> (effector memory) T-cell subsets (Figure S8B).

**Use of Encapsulated cGAMP and mKRAS to Treat Animals with Liver KPC Metastases.** To establish a liver metastasis model, a KRAS pancreatic cancer cell (KPC) line, derived from a transgenic Kras<sup>LSL</sup> G12D<sup>+</sup>/Trp53<sup>LSL</sup> R172H<sup>+</sup>/Pdx-1-Cre mouse model, was used for hemispleen injection, allowing spread to the liver via the portal vein (Figure 6A).<sup>63</sup> Briefly, murine spleens were surgically exposed under anesthesia, using two clips to divide the spleen in half (Figure 6A).<sup>39</sup> This was followed by injecting 10,000–50,000 KPC-luc into the splenic portion draining to the liver, followed by removal of the other half. Metastatic spread to the liver was followed by d-luciferin injection into the peritoneum and IVIS imaging. The number of injected KPC-luc cells was adjusted for the length of animal survival, established to be 16–22 days for 50,000 cells or 26–32 days for 10,000 cells. To study the therapeutic effect of cGAMP and mKRAS, 8-week-old female B6129SF1/J mice were randomly assigned to 5 groups, each including 8 animals. Following injection of 50,000 KPC-luc cells per animal (day 1), 4 therapeutic doses of cGAMP/LNP, mKRAS/LNP, cGAMP/mRAS<sup>WT</sup>/LNP, or cGAMP/mKRAS/LNP were IV injected on days 6, 9, 12, and 15 (Figure 7B). The dose of cGAMP was 0.3 mg/kg, and that of mKRAS or mRAS<sup>WT</sup> was 1.25 mg/kg per administration. Tumor growth was monitored by IVIS imaging on days 5, 11, 14, and 18, and body weights were recorded every 3 days. All mice were sacrificed on day 18 for blood collection and harvesting liver tissues for weighing and *ex vivo* IVIS imaging. Paraffin-embedded liver tissues were sectioned and stained with H&E or a fluorescent dye mixture (DAPI, anti-Ki67 antibody, and anti-CD8 antibody) for confocal microscopy. Additionally, the tissue slides were stained for perforin, IFN- $\gamma$ , FoxP3, and CD163 for IHC analysis. The sections were scanned by the Vectra Polaris Quantitative Pathology Imaging System. The blood was used for measuring serum IL-6 and IL-10 concentrations by ELISA according to the manufacturer's instructions.

**Prophylactic Administration of Encapsulated cGAMP and mKRAS to Determine the Effect on KPC Liver Metastasis.** Eight-week-old female B6129SF1/J mice were randomly assigned to 2 groups, each including 8 animals. Four doses of saline or cGAMP/mKRAS/LNP (0.3 mg/kg of cGAMP and 1.25 mg/kg of mKRAS) were IV injected into mice on days -14, -11, -7, and -4. On day 0, 50,000 KPC-luc cells were injected into the hemispleen as described above. An IVIS imaging system was used to monitor tumor growth on

days 7, 14, 21, and 28. The survival and weight of the mice were also recorded.

**Adoptive Cell Transfer.** Eight-week-old female B6129SF1/J mice were randomly assigned among 2 groups, with 3 animals in each group. Four IV administrations of saline or cGAMP/mKRAS/LNP (0.3 mg/kg of cGAMP and 1.25 mg/kg of mRNA) were delivered on days -21, -18, -14, -11. On day -7, all mice were euthanized to allow lymphocyte isolation from the spleen. The cells were used for adoptive transfer into recipient animals ( $n = 8$ ), each receiving  $3 \times 10^6$  lymphocytes IV. 50,000 KPC-luc cells were injected into the recipient hemispleens on day 21, and the IVIS imaging system was used to monitor metastatic growth on days 7, 14, 21, and 28. The results were displayed in Kaplan-Meier plots. We also assessed animal weight every 3 days.

**Biosafety Assessment.** Mice were treated with four IV administrations of PBS, free cGAMP, and cGAMP/mKRAS/LNP on days 1, 4, 7, and 10. The doses of cGAMP and mKRAS were 0.3 and 1.25 mg/kg, respectively. Serum was collected for the quantification of IL-6, TNF- $\alpha$ , ALT, AST, and BUN, and creatinine on days 2, 11, and 24.

**Statistics.** Comparative analysis of differences between groups was performed by 1-way ANOVA followed by Tukey's multiple comparisons. Values were expressed as mean  $\pm$  SD of multiple determinations. For all statistical analyses, a  $p$ -value of  $<0.05$  was considered statistically significant.

## ASSOCIATED CONTENT

### Data Availability Statement

All the data associated with this research has been included in the paper or the Supporting Information. Correspondence should be addressed to X.X. and A.E.N.

### Supporting Information

The Supporting Information is available free of charge at <https://pubs.acs.org/doi/10.1021/acsnano.4c14102>.

mRNA (mKRAS and mRAS<sup>WT</sup>) design; Parameters for LNP preparation; stability assay for cGAMP/mKRAS/LNP; hemolysis assay; activation of the STING pathway in KPC by encapsulated cGAMP; assessment of DC maturation *in vitro*; gating method to assess expression of CD80 in NPC; assessment of central and memory T-cells from spleen; impact of cGAMP/mKRAS/LNP treatment in mice with established pancreatic cancer liver metastasis; IHC staining for CD163 in liver slides; IVIS images of all survival experiments; *in vivo* biosafety assay (PDF)

## AUTHOR INFORMATION

### Corresponding Author

Andre E. Nel – Division of NanoMedicine, Department of Medicine, University of California, Los Angeles, California 90095, United States; California NanoSystems Institute, University of California, Los Angeles, California 90095, United States; [orcid.org/0000-0002-5232-4686](https://orcid.org/0000-0002-5232-4686); Email: [anel@mednet.ucla.edu](mailto:anel@mednet.ucla.edu)

### Authors

Xiao Xu – Division of NanoMedicine, Department of Medicine, University of California, Los Angeles, California 90095, United States; California NanoSystems Institute, University of California, Los Angeles, California 90095, United States; [orcid.org/0000-0003-0063-3468](https://orcid.org/0000-0003-0063-3468)

Xiang Wang – Division of NanoMedicine, Department of Medicine, University of California, Los Angeles, California 90095, United States; California NanoSystems Institute,

University of California, Los Angeles, California 90095, United States; [orcid.org/0000-0002-6647-0684](https://orcid.org/0000-0002-6647-0684)

Yu-Pei Liao – Division of NanoMedicine, Department of Medicine, University of California, Los Angeles, California 90095, United States; [orcid.org/0000-0001-7239-9426](https://orcid.org/0000-0001-7239-9426)

Lijia Luo – Division of NanoMedicine, Department of Medicine, University of California, Los Angeles, California 90095, United States; California NanoSystems Institute, University of California, Los Angeles, California 90095, United States; [orcid.org/0000-0001-7125-6562](https://orcid.org/0000-0001-7125-6562)

Complete contact information is available at: <https://pubs.acs.org/10.1021/acsnano.4c14102>

### Author Contributions

A.E.N. conceptualized the study, obtained the funding, and supervised the project and manuscript writing. The experimental planning was performed by X.X., with protocol assistance by X.W. and Y.P.L. The experiments were conducted by X.X., X.W., Y.P.L., and L.L., with data analysis by X.X. and X.W. X.X. wrote the original draft with the assistance of A.E.N. The final version was reviewed and edited by all authors.

### Funding

This study was supported by U.S. Public Health Service Grant R01CA247666–03 from the National Cancer Institute in the USA. We also acknowledge the generous support provided by the Marlin Miller, Jr. Family Foundation

### Notes

The authors declare the following competing financial interest(s): The authors declare the following financial and competing interests: Andre E. Nel is a co-founder and equity holder in Westwood Biosciences Inc. and Nammi Therapeutics. Andre E. Nel also serves on the Board for Westwood Biosciences Inc. The remaining authors declare no conflict of interest.

## ACKNOWLEDGMENTS

The authors thank the Electron Imaging Center for Nanomachines (EICN), the UCLA Flow Cytometry Core Facility, the Preclinical Imaging Technology Center, the Translational Pathology Core Laboratory (TPCL), the Molecular Instrumentation Center, and the CNSI Advanced Light Microscopy/Spectroscopy (ALMS) Shared Facility at UCLA. Yunfeng Li from TPCL helped with slide scanning and analysis. Salem Haile from the UCLA Flow Cytometry Core Facility helped set up the methods for flow cytometry analysis. Wong Hoi Hui from EICN helped with the cryoEM imaging and Chong Hyun Chang from the Nano and Pico Characterization Laboratory assisted in the characterization of LNP.

## REFERENCES

- (1) Halbrook, C. J.; Lyssiotis, C. A.; di Magliano, M. P.; Maitra, A. Pancreatic cancer: Advances and challenges. *Cell* **2023**, *186*, 1729–1754.
- (2) Franck, C.; Müller, C.; Rosania, R.; Croner, R. S.; Pech, M.; Venerito, M. Advanced Pancreatic Ductal Adenocarcinoma: Moving Forward. *Cancers* **2020**, *12*, 1955.
- (3) Gumberger, P.; Björnsson, B.; Sandström, P.; Bojmar, L.; Zambirinis, C. P. The Liver Pre-Metastatic Niche in Pancreatic Cancer: A Potential Opportunity for Intervention. *Cancers* **2022**, *14*, 3028.

- (4) Tsilimigras, D. I.; Brodt, P.; Clavien, P. A.; Muschel, R. J.; D'Angelica, M. I.; Endo, I.; Parks, R. W.; Doyle, M.; de Santibañes, E.; Pawlik, T. M. Liver metastases. *Nat. Rev. Dis. Primers* **2021**, *7*, 27.
- (5) Li, X.; Ramadori, P.; Pfister, D.; Seehawer, M.; Zender, L.; Heikenwalder, M. The immunological and metabolic landscape in primary and metastatic liver cancer. *Nat. Rev. Cancer* **2021**, *21*, 541–557.
- (6) Xu, X.; Wang, X.; Liao, Y. P.; Luo, L. J.; Xia, T.; Nel, A. E. Use of a Liver-Targeting Immune-Tolerogenic mRNA Lipid Nanoparticle Platform to Treat Peanut-Induced Anaphylaxis by Single- and Multiple-Epitope Nucleotide Sequence Delivery. *ACS Nano* **2023**, *17*, 4942–4957.
- (7) Poole, A.; Karupiah, V.; Hartt, A.; Haidar, J. N.; Moureau, S.; Dobrzycki, T.; Hayes, C.; Rowley, C.; Dias, J.; Harper, S.; et al. Therapeutic high affinity T cell receptor targeting a KRASG12D cancer neoantigen. *Nat. Commun.* **2022**, *13*, 5333.
- (8) Anthiya, S.; Öztürk, S. C.; Yanik, H.; Tavukcuoglu, E.; Şahin, A.; Datta, D.; Charisse, K.; Alvarez, D. M.; Loza, M. I.; Calvo, A.; Sulheim, E.; Loevenich, S.; Klinkenberg, G.; Schmid, R.; Manoharan, M.; Esendağlı, G.; Alonso, M. J. Targeted siRNA lipid nanoparticles for the treatment of KRAS-mutant tumors. *J. Controlled Release* **2023**, *357*, 67–83.
- (9) Yousef, A.; Yousef, M.; Chowdhury, S.; Abdilleh, K.; Knafl, M.; Edelkamp, P.; Alfaro-Munoz, K.; Chacko, R.; Peterson, J.; Smaglo, B. G.; et al. Impact of KRAS mutations and co-mutations on clinical outcomes in pancreatic ductal adenocarcinoma. *Npj Precis. Oncol.* **2024**, *8*, 27.
- (10) Palmer, D. H.; Valle, J. W.; Ma, Y. T.; Faluyi, O.; Neoptolemos, J. P.; Jensen Gjertsen, T.; Iversen, B.; Amund Eriksen, J.; Møller, A.-S.; Aksnes, A.-K.; Miller, R.; Dueland, S. TG01/GM-CSF and adjuvant gemcitabine in patients with resected RAS-mutant adenocarcinoma of the pancreas (CT TG01–01): a single-arm, phase 1/2 trial. *Br. J. Cancer* **2020**, *122*, 971–977.
- (11) Chaudhary, N.; Weissman, D.; Whitehead, K. A. mRNA vaccines for infectious diseases: principles, delivery and clinical translation. *Nat. Rev. Drug Discovery* **2021**, *20*, 817–838.
- (12) Wei, J.; Hui, A. M. The paradigm shift in treatment from COVID-19 to oncology with mRNA vaccines. *Cancer Treat. Rev.* **2022**, *107*, 102405.
- (13) Liu, C.; Shi, Q.; Huang, X.; Koo, S.; Kong, N.; Tao, W. mRNA-based cancer therapeutics. *Nat. Rev. Cancer* **2023**, *23*, 526–543.
- (14) Lorentzen, C. L.; Haanen, J. B.; Met, Ö.; Svane, I. M. J. T. L. O. Clinical advances and ongoing trials of mRNA vaccines for cancer treatment. *Lancet Oncol.* **2022**, *23*, No. e450–e458.
- (15) Zhou, L.; Yi, W.; Zhang, Z.; Shan, X.; Zhao, Z.; Sun, X.; Wang, J.; Wang, H.; Jiang, H.; Zheng, M. J. N. S. R. STING agonist-boosted mRNA immunization via intelligent design of nanovaccines for enhancing cancer immunotherapy. *Natl. Sci. Rev.* **2023**, *10*, nwad214.
- (16) Miao, L.; Li, L.; Huang, Y.; Delcassian, D.; Chahal, J.; Han, J.; Shi, Y.; Sadtler, K.; Gao, W.; Lin, J. J. N. B.; et al. Delivery of mRNA vaccines with heterocyclic lipids increases anti-tumor efficacy by STING-mediated immune cell activation. *Nat. Biotechnol.* **2019**, *37*, 1174–1185.
- (17) Lorentzen, C. L.; Haanen, J. B.; Met, Ö.; Svane, I. M. Clinical advances and ongoing trials on mRNA vaccines for cancer treatment. *Lancet Oncol.* **2022**, *23*, No. e450–e458.
- (18) Luo, L. J.; Wang, X.; Liao, Y. P.; Chang, C. H.; Nel, A. E. Nanocarrier Co-formulation for Delivery of a TLR7 Agonist plus an Immunogenic Cell Death Stimulus Triggers Effective Pancreatic Cancer Chemo-immunotherapy. *ACS Nano* **2022**, *16*, 13168–13182.
- (19) Yang, M.; Zhang, C. Y. The role of liver sinusoidal endothelial cells in cancer liver metastasis. *Am. J. Cancer Res.* **2021**, *11*, 1845–1860.
- (20) Yu, X.; Chen, L.; Liu, J.; Dai, B.; Xu, G.; Shen, G.; Luo, Q.; Zhang, Z. Immune modulation of liver sinusoidal endothelial cells by melittin nanoparticles suppresses liver metastasis. *Nat. Commun.* **2019**, *10*, 574.
- (21) Samson, N.; Ablasser, A. The cGAS-STING pathway and cancer. *Nat. Cancer* **2022**, *3*, 1452–1463.
- (22) Kwon, J.; Bakhoun, S. F. The Cytosolic DNA-Sensing cGAS-STING Pathway in Cancer. *Cancer Discovery* **2020**, *10*, 26–39.
- (23) Hendy, D. A.; Ma, Y.; Dixon, T. A.; Murphy, C. T.; Pena, E. S.; Carlock, M. A.; Ross, T. M.; Bachelder, E. M.; Ainslie, K. M.; Fenton, O. S. Polymeric cGAMP microparticles affect the immunogenicity of a broadly active influenza mRNA lipid nanoparticle vaccine. *J. Controlled Release* **2024**, *372*, 168–175.
- (24) Watkins-Schulz, R.; Batty, C. J.; Stiepel, R. T.; Schmidt, M. E.; Sandor, A. M.; Chou, W.-C.; Ainslie, K. M.; Bachelder, E. M.; Ting, J. P. Y. Microparticle Delivery of a STING Agonist Enables Indirect Activation of NK Cells by Antigen-Presenting Cells. *Mol. Pharmaceutics* **2022**, *19*, 3125–3138.
- (25) Huang, C.; Shao, N.; Huang, Y.; Chen, J.; Wang, D.; Hu, G.; Zhang, H.; Luo, L.; Xiao, Z. Overcoming challenges in the delivery of STING agonists for cancer immunotherapy: A comprehensive review of strategies and future perspectives. *Mater. Today Bio.* **2023**, *23*, 100839.
- (26) Dane, E. L.; Belessiotis-Richards, A.; Backlund, C.; Wang, J. N.; Hidaka, K.; Milling, L. E.; Bhagchandani, S.; Melo, M. B.; Wu, S. W.; Li, N.; Donahue, N.; Ni, K. Y.; Ma, L. Y.; Okaniwa, M.; Stevens, M. M.; Alexander-Katz, A.; Irvine, D. J. STING agonist delivery by tumour-penetrating PEG-lipid nanodiscs primes robust anticancer immunity. *Nat. Mater.* **2022**, *21*, 710–720.
- (27) Kim, M.; Jeong, M.; Hur, S.; Cho, Y.; Park, J.; Jung, H.; Seo, Y.; Woo, H. A.; Nam, K. T.; Lee, K.; et al. Engineered ionizable lipid nanoparticles for targeted delivery of RNA therapeutics into different types of cells in the liver. *Sci. Adv.* **2021**, *7*, No. eabf4398.
- (28) Zhang, X. W.; Bai, X. C.; Chen, Z. J. J. Structures and Mechanisms in the cGAS-STING Innate Immunity Pathway. *Immunity* **2020**, *53*, 43–53.
- (29) Zhu, W.; Wei, L.; Dong, C.; Wang, Y.; Kim, J.; Ma, Y.; Gonzalez, G. X.; Wang, B. Z. cGAMP-adjuvanted multivalent influenza mRNA vaccines induce broadly protective immunity through cutaneous vaccination in mice. *Mol. Ther. -Nucleic Acids* **2022**, *30*, 421–437.
- (30) Sun, X.; Zhang, Y.; Li, J.; Park, K. S.; Han, K.; Zhou, X.; Xu, Y.; Nam, J.; Xu, J.; Shi, X.; Wei, L.; Lei, Y. L.; Moon, J. J. Amplifying STING activation by cyclic dinucleotide–manganese particles for local and systemic cancer metalloimmunotherapy. *Nat. Nanotechnol.* **2021**, *16*, 1260–1270.
- (31) Yang, K.; Han, W.; Jiang, X.; Piffko, A.; Bugno, J.; Han, C.; Li, S.; Liang, H.; Xu, Z.; Zheng, W.; Wang, L.; Wang, J.; Huang, X.; Ting, J. P. Y.; Fu, Y.-X.; Lin, W.; Weichselbaum, R. R. Zinc cyclic di-AMP nanoparticles target and suppress tumours via endothelial STING activation and tumour-associated macrophage reinvigoration. *Nat. Nanotechnol.* **2022**, *17*, 1322–1331.
- (32) Wehbe, M.; Wang-Bishop, L.; Becker, K. W.; Shae, D.; Baljon, J. J.; He, X.; Christov, P.; Boyd, K. L.; Balko, J. M.; Wilson, J. T. Nanoparticle delivery improves the pharmacokinetic properties of cyclic dinucleotide STING agonists to open a therapeutic window for intravenous administration. *J. Controlled Release* **2021**, *330*, 1118–1129.
- (33) Koshy, S. T.; Cheung, A. S.; Gu, L.; Graveline, A. R.; Mooney, D. J. Liposomal Delivery Enhances Immune Activation by STING Agonists for Cancer Immunotherapy. *Adv. Biosys.* **2017**, *1*, 1600013.
- (34) Hao, M. X.; Zhu, L. L.; Hou, S. Y.; Chen, S. J.; Li, X. Q.; Li, K. M.; Zhu, N. C.; Chen, S. S.; Xue, L. J.; Ju, C. Y.; Zhang, C. Sensitizing Tumors to Immune Checkpoint Blockage via STING Agonists Delivered by Tumor-Penetrating Neutrophil Cytopharmaceuticals. *ACS Nano* **2023**, *17*, 1663–1680.
- (35) Decout, A.; Katz, J. D.; Venkatraman, S.; Ablasser, A. The cGAS-STING pathway as a therapeutic target in inflammatory diseases. *Nat. Rev. Immunol.* **2021**, *21*, 548–569.
- (36) Joffre, O. P.; Segura, E.; Savina, A.; Amigorena, S. Cross-presentation by dendritic cells. *Nat. Rev. Immunol.* **2012**, *12*, 557–569.
- (37) Cacicedo, M. L.; Medina-Montano, C.; Kaps, L.; Kappel, C.; Gehring, S.; Bros, M. J. C. Role of liver-mediated tolerance in nanoparticle-based tumor therapy. *Cells* **2020**, *9*, 1985.

- (38) Thomson, A. W.; Knolle, P. A. Antigen-presenting cell function in the tolerogenic liver environment. *Nat. Rev. Immunol.* **2010**, *10*, 753–766.
- (39) Soares, K. C.; Foley, K.; Olino, K.; Leubner, A.; Mayo, S. C.; Jain, A.; Jaffee, E.; Schulick, R. D.; Yoshimura, K.; Edil, B.; et al. A Preclinical Murine Model of Hepatic Metastases. *J. Vis. Exp.* **2014**, 51677.
- (40) Pimkova Polidarova, M.; Brehova, P.; Dejmek, M.; Birkus, G.; Brazdova, A. STING agonist-mediated cytokine secretion is accompanied by monocyte apoptosis. *ACS Infect. Dis.* **2022**, *8*, 463–471.
- (41) Sun, X.; Huang, X.; Park, K. S.; Zhou, X.; Kennedy, A. A.; Pretto, C. D.; Wu, Q.; Wan, Z.; Xu, Y.; Gong, W. Self-Assembled STING-Activating Coordination Nanoparticles for Cancer Immunotherapy and Vaccine Applications. *ACS Nano* **2024**, *18*, 10439–10453.
- (42) Luo, L.; Wang, X.; Liao, Y. P.; Chang, C. H.; Nel, A. E. Nanocarrier Co-formulation for Delivery of a TLR7 Agonist plus an Immunogenic Cell Death Stimulus Triggers Effective Pancreatic Cancer Chemo-immunotherapy. *ACS Nano* **2022**, *16*, 13168–13182.
- (43) Motedayen Aval, L.; Pease, J. E.; Sharma, R.; Pinato, D. J. Challenges and Opportunities in the Clinical Development of STING Agonists for Cancer Immunotherapy. *J. Clin. Med.* **2020**, *9*, 3323.
- (44) Su, T.; Zhang, Y.; Valerie, K.; Wang, X. Y.; Lin, S. B.; Zhu, G. Z. STING activation in cancer immunotherapy. *Theranostics* **2019**, *9*, 7759–7771.
- (45) Zheng, M. J.; Tian, Z. G. Liver-Mediated Adaptive Immune Tolerance. *Front. Immunol.* **2019**, *10*, 480451.
- (46) Dai, H. L.; Zheng, Y. W.; Thomson, A. W.; Rogers, N. M. Transplant Tolerance Induction: Insights From the Liver. *Front. Immunol.* **2020**, *11*, 1044.
- (47) Lu, L.; Barbi, J.; Pan, F. The regulation of immune tolerance by FOXP3. *Nat. Rev. Immunol.* **2017**, *17*, 703–717.
- (48) Li, F. L.; Tian, Z. G. The liver works as a school to educate regulatory immune cells. *Cell. Mol. Immunol.* **2013**, *10*, 292–302.
- (49) Shetty, S.; Lalor, P. F.; Adams, D. H. Liver sinusoidal endothelial cells — gatekeepers of hepatic immunity. *Nat. Rev. Gastroenterol. Hepatol.* **2018**, *15*, 555–567.
- (50) Carambia, A.; Gottwick, C.; Schwinge, D.; Stein, S.; Digigow, R.; Şeleci, M.; Mungalpara, D.; Heine, M.; Schuran, F. A.; Corban, C.; Lohse, A. W.; Schramm, C.; Heeren, J.; Herkel, J. Nanoparticle-mediated targeting of autoantigen peptide to cross-presenting liver sinusoidal endothelial cells protects from CD8 T-cell-driven autoimmune cholangitis. *Immunology* **2021**, *162*, 452–463.
- (51) Lu, D.; Chen, Y.; Jiang, M.; Wang, J.; Li, Y.; Ma, K.; Sun, W.; Zheng, X.; Qi, J.; Jin, W.; Chen, Y. KRAS G12V neoantigen specific T cell receptor for adoptive T cell therapy against tumors. *Nat. Commun.* **2023**, *14*, 6389.
- (52) Paunovska, K.; Da Silva Sanchez, A. J.; Lokugamage, M. P.; Loughrey, D.; Echeverri, E. S.; Cristian, A.; Hatit, M. Z. C.; Santangelo, P. J.; Zhao, K.; Dahlman, J. E. The Extent to Which Lipid Nanoparticles Require Apolipoprotein E and Low-Density Lipoprotein Receptor for Delivery Changes with Ionizable Lipid Structure. *Nano Lett.* **2022**, *22*, 10025–10033.
- (53) Yoon, J. H.; Jung, Y. J.; Moon, S. H. Immunotherapy for pancreatic cancer. *World J. Clin. Cases* **2021**, *9*, 2969–2982.
- (54) Chattopadhyay, S.; Liao, Y. P.; Wang, X.; Nel, A. E. Use of Stromal Intervention and Exogenous Neoantigen Vaccination to Boost Pancreatic Cancer Chemo-Immunotherapy by Nanocarriers. *Bioengineering* **2023**, *10*, 1205.
- (55) Garland, K. M.; Sheehy, T. L.; Wilson, J. T. Chemical and Biomolecular Strategies for STING Pathway Activation in Cancer Immunotherapy. *Chem. Rev.* **2022**, *122*, 5977–6039.
- (56) Biller, L. H.; Schrag, D. Diagnosis and Treatment of Metastatic Colorectal Cancer: A Review. *Jama-J. Am. Med. Assoc.* **2021**, *325*, 669–685.
- (57) Bear, A. S.; Nadler, R. B.; O’Hara, M. H.; Stanton, K. L.; Xu, C.; Saporito, R. J.; Rech, A. J.; Baroja, M. L.; Blanchard, T.; Elliott, M. H.; et al. Natural TCRs targeting KRAS G12V display fine specificity and sensitivity to human solid tumors. *J. Clin. Invest.* **2024**, *134*, No. e175790.
- (58) Cheng, Q.; Wei, T.; Farbiak, L.; Johnson, L. T.; Dilliard, S. A.; Siegwart, D. J. Selective organ targeting (SORT) nanoparticles for tissue-specific mRNA delivery and CRISPR-Cas gene editing. *Nat. Nanotechnol.* **2020**, *15*, 313–320.
- (59) Álvarez-Benedicto, E.; Tian, Z.; Chatterjee, S.; Orlando, D.; Kim, M.; Guerrero, E. D.; Wang, X.; Siegwart, D. J. Spleen SORT LNP Generated in situ CAR T Cells Extend Survival in a Mouse Model of Lymphoreplete B Cell Lymphoma. *Angew. Chem. Int. Ed.* **2023**, *62*, No. e202310395.
- (60) Chen, J.; Ye, Z.; Huang, C.; Qiu, M.; Song, D.; Li, Y.; Xu, Q. Lipid nanoparticle-mediated lymph node-targeting delivery of mRNA cancer vaccine elicits robust CD8 + T cell response. *Proc. Natl. Acad. Sci. U. S. A.* **2022**, *119*, No. e2207841119.
- (61) Rojas, L. A.; Sethna, Z.; Soares, K. C.; Olcese, C.; Pang, N.; Patterson, E.; Lihm, J.; Ceglia, N.; Guasp, P.; Chu, A.; Yu, R.; Chandra, A. K.; Waters, T.; Ruan, J.; Amisaki, M.; Zebboudj, A.; Odgerel, Z.; Payne, G.; Derhovanessian, E.; Müller, F.; Rhee, I.; Yadav, M.; Dobrin, A.; Sadelain, M.; Luksza, M.; Cohen, N.; Tang, L.; Basturk, O.; Gönen, M.; Katz, S.; Do, R. K.; Epstein, A. S.; Momtaz, P.; Park, W.; Sugarman, R.; Varghese, A. M.; Won, E.; Desai, A.; Wei, A. C.; D’Angelica, M. I.; Kingham, T. P.; Mellman, I.; Merghoub, T.; Wolchok, J. D.; Sahin, U.; Türeci, Ö.; Greenbaum, B. D.; Jarnagin, W. R.; Drebin, J.; O’Reilly, E. M.; Balachandran, V. P. Personalized RNA neoantigen vaccines stimulate T cells in pancreatic cancer. *Nature* **2023**, *618*, 144–150.
- (62) Akinc, A.; Maier, M. A.; Manoharan, M.; Fitzgerald, K.; Jayaraman, M.; Barros, S.; Ansell, S.; Du, X.; Hope, M. J.; Madden, T.; et al. The Onpattro story and the clinical translation of nanomedicines containing nucleic acid-based drugs. *Nat. Nanotechnol.* **2019**, *14*, 1084–1087.
- (63) Sangwan, V.; Banerjee, S.; Jensen, K. M.; Chen, Z.; Chugh, R.; Dudeja, V.; Vickers, S. M.; Saluja, A. K. Primary and Liver Metastasis-Derived Cell Lines From KrasG12D; Trp53R172H; Pdx-1 Cre Animals Undergo Apoptosis in Response to Triptolide. *Pancreas* **2015**, *44*, 583–589.